Summary of a Doctoral Thesis

Design of Composite Pulse Sequences for Quantum Tecnnologies

Author:
Hayk L. Gevorgyan

Supervisor:
Acad. Prof. DSc.
Nikolay V. Vitanov

Summary of a thesis submitted in fulfillment
of the requirements for the degree of
Doctor of Philosophy

Department of Theoretical Physics
Group of Quantum Optics and Quantum Information

Sofia University St. Kliment Ohridski
Sofia, Bulgaria

May 2023

Author:
Hayk L. Gevorgyan

Supervisor:
Acad. Prof. DSc. Nikolay V. Vitanov

Institute:
Sofia University St. Kliment Ohridski, Sofia, Bulgaria

CONTENTS

LIST OF FIGURES

LIST OF TABLES

ABSTRACT

Composite pulses occupies an honorable place in the range of quantum control techniques, and has an advantage among them to be suitable for robust, sensitive or any high-precision manipulation of quantum systems. The goal is to expand the scope of the methodology born in nuclear magnetic resonance, and modernize its applications. We present the leverage of this flexible method in quantum computing, quantum sensing, quantum information processing, and polarization optics. The latter point to the existence of a quantum-classical analogy due to the underlying analogous mathematics.

The possibility to design robust quantum gates via broadband composite pulses with ultrahigh-fidelity exceeding the quantum computation benchmark is remarkable for quantum computing. Derivation of the narrowband and passband composite pulses for quantum sensing applications imposes the use of SU(2) and novel regularization approaches of optimization. Interestingly, composite pulses is also capable of robust transitions of ultrasmall probability, and can have potential applications to deterministic single-photon emission and the DLCZ protocol well-known in quantum information processing. Another modification leads to ultrarobust and ultrasensitive quantum controls of transition probability via composite pulses, which may have essential applications for creation of ultrabroadband and ultranarrowband conversion efficiency polarization half-wave plates. Also the similar optimization method can be applied to design ultrarobust Z quantum gates, equivalent to polarization π rotators in polarization optics. Composite pulses parameters can be utilised for construction of broadband composite nonreciprocal polarization wave plates and optical isolators.

We cover a wide range of research disciplines and provide a deep and broad understanding of the interdisciplinarity, flexibility and possibilities of the technique. In this sense, composite pulses is powerful and has great prospects.

STATEMENT OF AUTHORSHIP

I, Hayk L. Gevorgyan, born November 27, 1995 in Yerevan, Armenia, declare that this thesis titled *Design of Composite Pulse Sequences for Quantum Tecnnologies* and the work presented in it are my own. I confirm that this work was done mainly while in candidature for a research degree at Sofia Universiy St. Kliment Ohridski.

Except where reference is made in the text of the thesis, this thesis contains no material published elsewhere or extracted in whole or in part from a thesis accepted for the award of any other degree or diploma. No other person's work has been used without due acknowledgment in the main text of the thesis. This thesis has not been submitted for the award of any degree or diploma in any other tertiary institution.

Hayk L. Gevorgyan May 24, 2023

ACKNOWLEDGMENTS

I wish to thank the H2020-MSCA-ITN-ETN (Horizon 2020 - Marie Skłodowska-Curie actions - Innovative Training Networks - European Training Networks), *Light-Matter Interfaces for Quantum Enhanced Technologies* project (LIMQUET - Contract No. 765075), funded by the European Commission, for the financial support.

I express my sincere gratitude to my supervisor **Acad. Prof. DSc. Nikolay V. Vitanov** for his professional guide during my Ph.D. study. It was an honor for me to get to know him and the members of his group *Quantum Optics and Quantum Information*, in the department of theoretical physics at the University of Sofia. Thank you all of you for fruitful discussions and support.

I would like to thank Prof. Stéphane Guerin for inviting me to the project after my master's degree at the Université Bourgogne-Franche-Comté, Dijon, France, and for welcoming and supervising me during my secondment in his laboratory.

DEDICATION

to my father-scientist Lekdar A. Gevorgian and mother-scientist Anahit H. Shamamian

ACRONYMS

CP	Composite Pulse
CPs	Composite Pulses
NMR	Nuclear Magnetic Resonance
PO	Polarization Optics
QC	Quantum Computing
QI	Quantum Information
QIP	Quantum Information Processing
QS	Quantum Sensing

1 INTRODUCTION

1.1 QUANTUM COHERENT CONTROL TECHNIQUES

A huge variety of quantum control techniques are used in many areas of physics to manipulate the physical system. Among them few are appreciable as resonant excitation, adiabatic passage, shaped pulses, optimal control theory, Composite Pulses (CPs). It is also entertaining that they can be adapted to obtain new control methods such as composite adiabatic passage and shortcut to adiabaticity. In general, coherent control techniques differ from each other by the choice of targeted cost parameters, hence, the resulting quality indicators are different.

1.2 ROTATIONS ON THE BLOCH SPHERE

The propagator of a coherently driven qubit is the solution of the Schrödinger equation,

$$i\hbar\partial_t \mathbf{U}(t,t_i) = \hat{H}(t)\mathbf{U}(t,t_i), \tag{1.1}$$

subject to the initial condition $\mathbf{U}(t_i,t_i) = \hat{I}$, the identity matrix. If the Hamiltonian is Hermitian, the propagator is unitary. If the Hamiltonian is also traceless, then the propagator has the SU(2) symmetry and can be represented as

$$\mathbf{U}_0 = \begin{bmatrix} a & b \\ -b^* & a^* \end{bmatrix}, \tag{1.2}$$

where a and b are the complex-valued Cayley-Klein parameters satisfying $|a|^2 + |b|^2 = 1$. A traceless Hermitian Hamiltonian has the form $\hat{H}(t) = \frac{1}{2}\hbar[\Omega(t)\cos(\phi)\hat{\sigma}_x + \Omega(t)\sin(\phi)\hat{\sigma}_y + \Delta\hat{\sigma}_z]$, where $\Omega(t)$ (assumed real and positive) is the Rabi frequency quantifying the coupling, ϕ is its phase, and Δ is the field-system detuning.

On exact resonance ($\Delta = 0$) and for $\phi = 0$, we have $a = \cos(A/2)$, $b = -i\sin(A/2)$, where A is the temporal pulse area $A = \int_{t_i}^{t_f} \Omega(t)\,\mathrm{d}t$. For a system starting in state $|1\rangle$, the single-pulse transition probability is $p = |b|^2 = \sin^2(A/2)$.

1.2.1 *Rotation gate*

Each pulse in a Composite Pulse (CP) sequence is considered resonant and hence it generates the propagator

$$\mathbf{U}(A,\phi) = \begin{bmatrix} \cos(A/2) & -ie^{i\phi}\sin(A/2) \\ -ie^{-i\phi}\sin(A/2) & \cos(A/2) \end{bmatrix}, \tag{1.3}$$

where ϕ is the phase of the coupling.

Our objective is to construct the qubit rotation gate $\hat{R}_y(\theta) = e^{i(\theta/2)\hat{\sigma}_y}$, where θ is the rotation angle and $\hat{\sigma}_y$ is the Pauli's y matrix. In matrix form,

$$\mathbf{R}_y(\theta) = \begin{bmatrix} \cos(\theta/2) & \sin(\theta/2) \\ -\sin(\theta/2) & \cos(\theta/2) \end{bmatrix}. \tag{1.4}$$

The X or NOT gate is defined as

$$\mathbf{X} = \begin{bmatrix} 0 & 1 \\ -1 & 0 \end{bmatrix}. \tag{1.5}$$

We shall use the following form of the Hadamard gate (known as pseudo-Hadamard form),

$$\mathbf{H} = \mathbf{R}_y(\pi/2) = e^{i(\pi/4)\hat{\sigma}_y} = \frac{1}{\sqrt{2}}\begin{bmatrix} 1 & 1 \\ -1 & 1 \end{bmatrix}. \tag{1.6}$$

A single resonant pulse of temporal area $A = \theta_\epsilon = \theta(1+\epsilon)$ produces the propagator $\hat{R}(\theta_\epsilon) = e^{i[\theta(1+\epsilon)/2]\hat{\sigma}_y} = \hat{R}(\theta)[1+O(\epsilon)]$, i.e. it is accurate up to zeroth order $O(\epsilon^0)$ in the pulse area error ϵ. Our approach is to replace the single θ pulse with a CP sequence of pulses of appropriate pulse areas and phases, such that the overall propagator produces the rotation gate (1.4) with an error of higher order, i.e. $\hat{R}(\theta)[1+O(\epsilon^{n+1})]$. Then we say that the corresponding composite rotation gate is accurate up to, and including, order $O(\epsilon^n)$.

1.2.2 *Phase-shift gate*

A phase-shift gate (up to a global phase factor) is defined as

$$\mathbf{F}(\phi) = \mathbf{R}_z(\phi) = \begin{bmatrix} e^{-i\phi/2} & 0 \\ 0 & e^{i\phi/2} \end{bmatrix} := \begin{bmatrix} 1 & 0 \\ 0 & e^{i\phi} \end{bmatrix}. \tag{1.7}$$

It cannot be obtained via a single theta pulse (5.1), and thus requires a circuit with two or more $\theta = \pi$ rotation gates

$$\mathbf{F}(\phi) = \mathbf{U}(\pi, \nu + \pi - \phi/2)\mathbf{U}(\pi, \nu) = \mathbf{U}(\pi, \nu)\mathbf{U}(\pi, \nu + \pi + \phi/2). \tag{1.8}$$

1.3 COMPOSITE PULSES IN NUCLEAR MAGNETIC RESONANCE

CPs have been developed in Nuclear Magnetic Resonance (NMR) in the 1980s. However, similar ideas have been introduced in Polarization Optics (PO) much earlier, in the 1940s [1–4]: by stacking several ordinary wave plates at specific angles with respect to their fast polarization axes one can design either achromatic (broadband) polarization retarders and rotators or (narrowband) polarization filters [1–10]. In the last two decades, CPs have spread out to most experimental Quantum Information (QI) platforms far beyond NMR. Applications include qubit control in trapped ions [11–18], neutral atoms [19], doped solids [20–22], quantum dots [23–28], and NV centers in diamond [29], high-accuracy optical clocks [30], cold-atoms interferometry [31–33], optically dense atomic ensembles [34], magnetometry [35], optomechanics [36], etc.

CPs are classified in NMR by Wimperis [37] into broadband, narrowband and passband classes, where he defined 1^{st} type and 2^{nd} type of pulses BB_1, NB_1, PB_1 and BB_2, NB_2, PB_2 respectively.

BB_1 and BB_2 pulses follow

$$BB_1(\theta) : (\pi)_{\phi_1}(2\pi)_{\phi_2}(\pi)_{\phi_1}(\theta)_0, \tag{1.9}$$

with $\phi_1 = \arccos(-\theta/4\pi)$ and $\phi_2 = 3\phi_1$,

$$BB_2(\theta) : (\pi)_{\pi/2}(2\pi)_{\phi_2}(\pi)_{\pi/2}(\theta)_0, \tag{1.10}$$

with $\phi_2 = 3\pi/2 + \theta/4$.

NB_1 and NB_2 pulses follow

$$NB_1(\theta) : (\pi)_{\phi_1}(2\pi)_{\phi_2}(\pi)_{\phi_1}(\theta)_0, \tag{1.11}$$

with $\phi_1 = \arccos(-\theta/4\pi)$ and $\phi_2 = -\phi_1$,

$$NB_2(\theta) : (\pi)_{\pi/2}(2\pi)_{\phi_2}(\pi)_{\pi/2}(\theta)_0, \tag{1.12}$$

with $\phi_2 = 3\pi/2 - \theta/4$.

NB_1 and NB_2 pulses follow

$$PB_1(\theta) : (2\pi)_{\phi_1}(4\pi)_{\phi_2}(2\pi)_{\phi_1}(\theta)_0, \tag{1.13}$$

with $\phi_1 = \arccos(-\theta/8\pi)$ and $\phi_2 = -\phi_1$,

$$PB_2(\theta) : (2\pi)_{\pi/2}(4\pi)_{\phi_2}(2\pi)_{\pi/2}(\theta)_0, \tag{1.14}$$

with $\phi_2 = 3\pi/2 - \theta/8$.

Besides these asymmetric sequences, Jones and co-workers [38] develop time-symmetric sequence called SCROFULOUS (Short composite rotation for undoing length over and under shoot),

$$SCROFULOUS(\theta) : (\theta_1)_{\phi_1}(\pi)_{\phi_2}(\theta_1)_{\phi_1}, \tag{1.15}$$

with $\theta_1 = \text{arcsinc}(2\cos(\theta/2)/\pi)$, $\phi_1 = \arccos(-\pi\cos\theta_1/(2\theta_1\sin\theta/2))$, $\phi_2 = \phi_1 - \arccos(-\pi/2\theta_1)$, where unnormalized sinc function is defined as $\text{sinc}(\theta) = \sin\theta/\theta$.

In the case of π rotation, one can choose $\theta_1 = \text{arcsinc}(0) = \pi$ and $\arccos(-\pi/2\theta_1) = -4\pi/3$,

$$SCROFULOUS(\pi) : (\pi)_{\pi/3}(\pi)_{5\pi/3}(\pi)_{\pi/3}. \tag{1.16}$$

Thus $\phi_2 - \phi_1 = 4\pi/3$, and Tycko's and co-workers' [39] result can be recovered

$$Tycko(N = 3) : (\pi)_0(\pi)_{2\pi/3}(\pi)_0, \tag{1.17}$$

for the broadband excitation without phase distortion. This leads to the division of the broadband CPs into two sub-classes, named variable and constant rotations [40–42].

SCROFULOUS is the shortest constant rotation with the first order of pulse area error compensation. BB_1 is the second order constant rotation, which is outperformed by our shorter X5 and H5s symmetric sequences [43].

SK1 is the shortest passband CP [44], being geometric rotation gate [45], as SCROFULOUS, also consists of three elementary pulses

$$SK1 : (\theta)_0(2\pi)_{\phi_1}(2\pi)_{-\phi_1}, \tag{1.18}$$

with parameter $\phi_1 = \arccos(-\theta/4\pi)$.

In this thesis we propose analytical and numerical methods for systematic derivation of CPs, to obtain the required property with better trade-off between operation run-time and property measure.

1.4 THESIS OUTLINE

The remainder of this thesis is organized as follows. Chapter 1 provides background information relevant to the field of research, viz., a detailed discussion of the major existing contributions of CPs technique in the literature. Chapter 2 details the application of the technique into Quantum Computing (QC), especially for the design of ultrahigh-fidelity composite rotation gates [43]. Chapter 3 details the application of the technique for the design of ultrahigh-fidelity composite phase gates [46] with the same method in QC. Chapter 4 summarizes the results of narrowband and passband CP sequences, applicable to Quantum Sensing (QS). Chapter 5 modernizes the properties of the technique, opening new horizons for the development of robust ultrasmall probability transitions with the application to deterministic single-photon emission in Quantum Information Processing (QIP). Chapter 6 examines the capability of the technique for ultrarobust or ultrasensitive control. These novel CPs are suitable for PO applications such as ultrabroadband and ultranarrowband composite polarization half waveplates [47]. Chapter 7 presents the use of the methodology for the development of optical devices, namely broadband nonreciprocal polarization waveplates and optical isolators [48] in PO. Chapter 8 concludes this thesis.

2

COMPOSITE PULSES FOR ROBUST ULTRAHIGH-FIDELITY ROTATION GATES

2.1 INTRODUCTION

Various proposals have been made in order to generate rotation gates that are resilient to experimental errors, at the expense of being longer, and hence slower. Adiabatic techniques are the traditional remedy for tackling such errors [49] — adiabatic evolution via a half crossing [50–58], half-SCRAP (Stark-chirped rapid adiabatic passage) [54], two-state STIRAP (stimulated Raman adiabatic passage) [55–57, 59]. An extension of this half-crossing technique to three states has been experimentally demonstrated in a trapped-ion experiment, with an error of about 1.4×10^{-4}, i.e. close to the quantum computation benchmark level [58], which was achieved by using pulse shaping. Another proposal used a sequence of two half-crossing adiabatic pulses split by a phase jump, which serves as a control parameter to the created superposition state [60].

In three-state Raman-coupled qubits, a very popular technique is fractional STIRAP [61–63] and leads to the creation of a coherent superposition of the two end states of the chain. Tripod-STIRAP [64–66], an extension of STIRAP has also been used for the generation of coherent superpositions of these three states or two of them. We also note quantum Householder reflections [67, 68].

A powerful alternative to achieve ultrahigh fidelity while featuring robustness to parameter errors is the technique of CPs [40, 41]. The CP sequence is a finite train of pulses with well-defined relative phases between them. These phases are control parameters, which are determined by the desired excitation profile. CPs can shape the excitation profile in essentially any desired manner, which is impossible with a single resonant pulse or adiabatic techniques. In particular, one can create a broadband composite π pulse, which delivers transition probability of 1 not only for a pulse area $A = \pi$ and zero detuning $\Delta = 0$, as a single resonant π pulse, but also in some ranges around these values [20, 37, 40, 41, 69–77]. Alternatively, narrowband CPs [37, 42, 73, 75, 78–83] squeeze the excitation profile around a certain point in the para-

meter space: they produce excitation that is more sensitive to parameter variations than a single pulse, with interesting applications to sensing, metrology and spatial localization. A third family of CPs — passband pulses — combine the features of broadband and narrowband pulses: they provide highly accurate excitation inside a certain parameter range and negligibly small excitation outside it [37, 82, 84–87].

CPs have been developed in NMR in the 1980's. In the last two decades, CPs have spread out to most experimental QI platforms far beyond NMR. Applications include qubit control in trapped ions [11–18], neutral atoms [19], doped solids [20–22], quantum dots [23–28], and NV centers in diamond [29], high-accuracy optical clocks [30], cold-atoms interferometry [31–33], optically dense atomic ensembles [34], magnetometry [35], optomechanics [36], etc.

CPs are particularly suitable for QI because they are quite unique in providing both ultrahigh fidelity and resilience to experimental errors. No other quantum control method offers this combination of high fidelity and robustness to errors and therefore, CPs might be the key enabling control technology for high-fidelity qubit operations which are mandatory in scalable QC.

In this chapter, we present several sets of single-qubit rotation quantum gates constructed with CP sequences. *Constant-rotation*, or *phase-distortionless* [39], CPs (sometimes called *Class A*) are obviously more demanding and require longer sequences, with respect to *variable-rotation* CPs, for the same order of compensation. However, in QIP wherein phase relations are essential, constant rotations are clearly the ones to be used for quantum rotation gates [38].

In this chapter, we focus at the derivation of ultrahigh-fidelity composite rotation gates, including the X, Hadamard and general rotation, which compensate pulse-area errors up to eighth order. Our results extend earlier results on some of these gates using shorter pulse sequences. The first phase-distortionless CP was designed by Tycko [78] which produces a composite X gate. A second-order error compensation CP was constructed by Wimperis, the well-known BB1 (broadband of type 1) pulse [37, 74]. Jones and co-workers have devoted a great deal of attention to composite X gates, with an emphasis of geometric approaches for derivation of such sequences, which work up to 5 and 7 pulses [38, 88–90]. We point out that our results supplement earlier results by our and other groups on different gates, i.e. composite quantum phase gate [91], the CNOT [92–98], Toffoli [99], and C^n-NOT gates [99].

Composite rotation gates have been constructed using nesting and concatenation of shorter composite sequences, and for larger error order, this procedure produces (impractical) composite sequences of extreme length. Here we use analytic approaches and brute-force numerics to derive rotation gates with much shorter sequences than before.

This chapter is organized as follows. In Sec. 2.2 we explain the derivation method. Composite π rotations, representing the X gate are presented in Sec. 2.3. Composite implementations of the Hadamard gate are given in Sec. 2.4, and composite rotation gates in Sec. 2.5. Finally, Sec. 2.6 presents the conclusions.

2.2 SU(2) APPROACH

The derivation of the composite rotation gates is done in the following manner. A phase shift ϕ imposed on the driving field, $\Omega(t) \to \Omega(t)\,\mathrm{e}^{i\phi}$, is imprinted onto the propagator (1.2) as

$$\mathbf{U}_\phi = \begin{bmatrix} a & b\,\mathrm{e}^{i\phi} \\ -b^*\,\mathrm{e}^{-i\phi} & a^* \end{bmatrix}. \tag{2.1}$$

A train of N pulses, each with area A_k and phase ϕ_k (applied from left to right),

$$(A_1)_{\phi_1}(A_2)_{\phi_2}(A_3)_{\phi_3}\cdots(A_N)_{\phi_N}, \tag{2.2}$$

produces the propagator (acting, as usual, from right to left)

$$\mathcal{U} = \mathbf{U}_{\phi_N}(A_N)\cdots\mathbf{U}_{\phi_3}(A_3)\mathbf{U}_{\phi_2}(A_2)\mathbf{U}_{\phi_1}(A_1). \tag{2.3}$$

Let us assume that the nominal (i.e. for zero error) pulse areas A_k have a systematic error ϵ, i.e. $A_k \to A_k(1+\epsilon)$.

Our objective in this chapter is to construct the qubit rotation gate $\hat{R}_y(\theta) = e^{i(\theta/2)\hat{\sigma}_y}$ (1.4). Under the assumption of a single systematic pulse area error ϵ, we can expand the composite propagator (2.3) in a Taylor series versus ϵ. Because of the SU(2) symmetry of the overall propagator, it suffices to expand only two of its elements, say $\mathcal{U}_{11}(\epsilon)$ and $\mathcal{U}_{12}(\epsilon)$. We set their zero-error values to the target values,

$$\mathcal{U}_{11}(0) = \cos(\theta/2), \quad \mathcal{U}_{12}(0) = \sin(\theta/2), \tag{2.4}$$

and we set as many of their derivatives with respect to ϵ, in the increasing order, as possible,

$$\mathcal{U}_{11}^{(m)}(0) = 0, \quad \mathcal{U}_{12}^{(m)}(0) = 0, \quad (m = 1, 2, \ldots, n), \tag{2.5}$$

where $\mathcal{U}_{jl}^{(m)} = \partial_\epsilon^m \mathcal{U}_{jl}$ denotes the mth derivative of $\mathcal{U}_{jl}$ with respect to ϵ. The largest derivative order n satisfying Eqs. (2.5) gives the order of the error compensation $O(\epsilon^n)$.

2.2.1 *Quantum gate fidelity*

If Eqs. (2.4) and (2.5) are satisfied, then the overall propagator can be written as

$$\mathcal{U}(\epsilon) = \mathbf{R}(\theta) + O(\epsilon^{n+1}), \tag{2.6}$$

with $\mathbf{R}(\theta) = \mathcal{U}(0)$. Then the *Frobenius distance fidelity*,

$$\mathcal{F} = 1 - \|\mathcal{U}(\epsilon) - \mathbf{R}(\theta)\| = 1 - \sqrt{\tfrac{1}{4}\sum_{j,k=1}^{2} \left|\mathcal{U}_{jk} - R_{jk}\right|^2}, \tag{2.7}$$

is of the same error order $O(\epsilon^n)$ as the propagator, $\mathcal{F} = 1 - O(\epsilon^{n+1})$. As shown by Jones and co-workers [100] for the composite X gates, the *trace fidelity*,

$$\mathcal{F}_{\mathrm{T}} = \tfrac{1}{2}\mathrm{Tr}\left[\mathcal{U}(\epsilon)\mathbf{R}(\theta)^{\dagger}\right], \tag{2.8}$$

has a factor of 2 higher error order $O(\epsilon^{2n})$, i.e. $\mathcal{F}_{\mathrm{T}} = 1 - O(\epsilon^{2n+1})$. Throughout this chapter we shall use the Frobenius distance fidelity (2.7), which is a much more strict and unforgiving to errors fidelity measure; moreover, its error is of the same order as the propagator error.

2.2.2 *Composite pulse sequences*

We have performed extensive numeric simulations which have returned numerous solutions. We have categorized them in three types of composite sequences, one symmetric and two asymmetric.

- Each symmetric sequence consists of a sequence of $2n-1$ nominal π pulses, sandwiched by two pulses of areas α, with symmetrically ordered phases,

$$\alpha_{\phi_1}\pi_{\phi_2}\pi_{\phi_3}\cdots\pi_{\phi_{n-1}}\pi_{\phi_n}\pi_{\phi_{n-1}}\cdots\pi_{\phi_3}\pi_{\phi_2}\alpha_{\phi_1}. \tag{2.9}$$

  These sequences generalize the three-pulse SCROFULOUS sequence [38], which is of this type, to more than three pulses.

- The first type of asymmetric sequences consists of a sequence of nominal π pulses, preceded (or superseded) by a pulse of area θ,

$$\pi_{\phi_1}\pi_{\phi_2}\pi_{\phi_3}\cdots\pi_{\phi_{N-1}}\theta_{\phi_N}. \tag{2.10}$$

  These sequences generalize the five-pulse BB1 sequence [37], which is of this type, to more than five pulses.

- The second type of asymmetric sequences consists of a sequence of $N-2$ nominal π pulses, preceded (or superseded) by single pulses of areas α and β,

$$\alpha_{\phi_1}\pi_{\phi_2}\pi_{\phi_3}\cdots\pi_{\phi_{N-1}}\beta_{\phi_N}. \tag{2.11}$$

  To the best of our knowledge, this type of composite sequences has not been reported in the literature hitherto.

2.3 X (NOT) GATE

As it is well known, such a gate (1.5) can be produced by a resonant pulse of temporal area π. The Frobenius distance fidelity (2.7) reads

$$\mathcal{F} = 1 - \sqrt{2}\left|\sin\frac{\pi\epsilon}{4}\right|. \tag{2.12}$$

For comparison, the trace fidelity is

$$\mathcal{F}_T = 1 - 2\sin^2\frac{\pi\epsilon}{4} = \cos\frac{\pi\epsilon}{2}. \tag{2.13}$$

The three types of composite sequences (5.33), (2.10), and (2.11) coalesce into a single type, a sequence of π pulses. Below we consider these sequences, in the increasing order of error compensation.

2.3.1 *First-order error compensation*

The careful analysis of Eqs. (2.4) and (2.5) shows that the shortest possible CP which can compensate first-order errors consists of three pulses, each with a pulse area of π, and symmetric phases,

$$\pi_{\phi_1}\pi_{\phi_2}\pi_{\phi_1}. \tag{2.14}$$

Solving Eq. (2.4) along with Eq. (2.5) for the first derivatives gives two solutions for the phases,

$$\pi_{\frac{1}{6}\pi}\pi_{\frac{5}{6}\pi}\pi_{\frac{1}{6}\pi}, \tag{2.15a}$$

$$\pi_{\frac{5}{6}\pi}\pi_{\frac{1}{6}\pi}\pi_{\frac{5}{6}\pi}. \tag{2.15b}$$

These two sequences generate the same propagator and hence the same fidelity.

2.3.2 *Second-order error compensation*

For sequences of four pulses, it becomes possible to annul the second-order derivatives in Eq. (2.5). A number of solutions exist, some of which are

$$(2\pi)_{3\chi}\pi_{\pi+\chi}\pi_{\frac{1}{2}\pi}\pi_{-\chi}, \tag{2.16a}$$

$$\pi_{\pi+\chi}(2\pi)_{3\chi}\pi_{\pi+\chi}\pi_{\frac{1}{2}\pi}, \tag{2.16b}$$

$$\pi_{\frac{1}{2}\pi}\pi_{\pi+\chi}(2\pi)_{3\chi}\pi_{\pi+\chi}, \tag{2.16c}$$

$$\pi_{-\chi}\pi_{\frac{1}{2}\pi}\pi_{\pi+\chi}(2\pi)_{3\chi}, \tag{2.16d}$$

where $\chi = \arcsin\left(\frac{1}{4}\right) \approx 0.0804\pi$. The second and third sequences are related to the BB1 sequence of Wimperis [37]. Note that all these sequences have a total nominal pulse area of 5π, and can be considered as five-pulse sequences because the effect of $(2\pi)_{3\chi}$ is the same as $\pi_{3\chi}\pi_{3\chi}$.

We have derived also the symmetric sequence

$$\pi_{\phi_1}\pi_{\phi_2}\pi_{\phi_3}\pi_{\phi_2}\pi_{\phi_1}, \tag{2.17}$$

with $\phi_1 = \arcsin\left(1-\sqrt{5/8}\right) \approx 0.0672\pi$, $\phi_2 = \arcsin\left((3\sqrt{10}-2)/8\right) \approx 0.3854\pi$, $\phi_3 = 2\phi_2 - 2\phi_1 + \pi/2 \approx 1.1364\pi$.

We conclude this subsection by noting that the availability of various four- and five-pulse symmetric and asymmetric sequences which produce the same fidelity is not a redundancy because they may have rather different sensitivity to phase errors, as has been shown recently for other composite sequences [101].

2.3.3 *Higher-order error compensation*

The $2n+1$-pulse sequences have an additional free phase which can be used to make the composite sequence *symmetric* as in Eq. (5.33), viz.

$$\pi_{\phi_1}\pi_{\phi_2}\pi_{\phi_3}\cdots\pi_{\phi_{n-1}}\pi_{\phi_n}\pi_{\phi_{n-1}}\cdots\pi_{\phi_3}\pi_{\phi_2}\pi_{\phi_1}. \tag{2.18}$$

Eqs. (2.4) and (2.5) reduce to a set of $n+1$ real trigonometric equations for $n+1$ free phases. There are multiple solutions for the phases for every $(2n+1)$-pulse composite sequence.

We have derived numerically the composite phases of symmetric sequences of an odd number of pulses, Eq. (2.18). They are presented in Table 2.1 in the main thesis The fidelity of these composite X gates is plotted in Figure 2.1. It is clear from the table

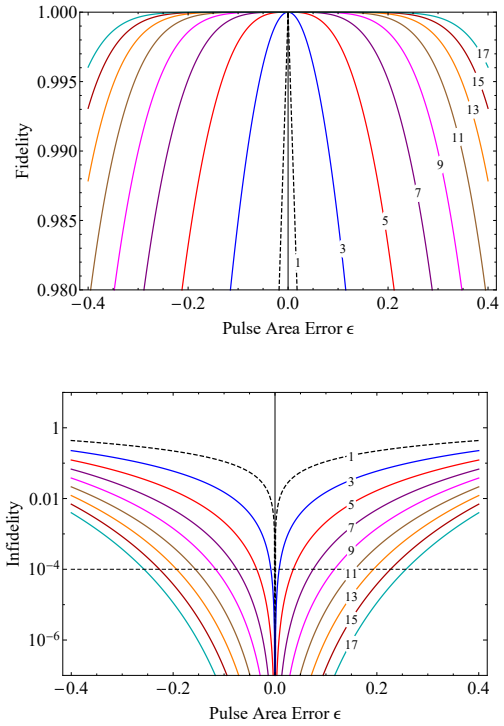

Figure 2.1: Frobenius distance fidelity F (top) and infidelity (bottom) of composite X gates. The infidelity is in logarithmic scale in order to better visualize the high-fidelity (low-infidelity) range. The numbers N on the curves refer to composite sequences XN listed in Table 2.1 in the main thesis.

and the figure that a single pulse has very little room for errors as the high-fidelity X gate allows for pulses area errors of less than 0.01%. The three-pulse composite X gate offers some leeway, with the admissible error of 0.8%. The real pulse area error correction effect is achieved with the composite sequences of 5 to 9 pulses, for which the high-fidelity range of admissible errors increases from 3.6% to 11.7%. Quite remarkably, errors of up to 25% can be eliminated, and ultrahigh fidelity maintained, with the 17-pulse composite X gate. Note that these error ranges are calculated by using the rather tough Frobenius distance fidelity (2.7). Had we use the much more relaxed trace distance fidelity (2.8), these ranges would be much broader, see the numbers for 1, 3 and 5 pulses above.

2.4 HADAMARD GATE

The Hadamard gate (1.6) can be generated by an ideal resonant $\pi/2$ pulse, which is, however, prone to experimental errors. In order to construct the composite Hadamard gate we have considered all three types of composite sequences (5.33), (2.10), and (2.11). Below we consider these sequences, in the increasing order of error compensation.

2.4.1 *First-order error correction*

The shortest pulse sequence that can provide a first-order error compensated Hadamard gate consists of three pulses,

$$\alpha_{\phi_1}\pi_{\phi_2}\alpha_{\phi_1}. \tag{2.19}$$

The value of the pulse area α is given by an inverse sinc function of $\sqrt{2}/\pi$, which gives $\alpha \approx 0.6399\pi$. Given α, we can find $\phi_1 - \phi_2$. The values are $\phi_1 \approx 1.8442\pi$ and $\phi_2 \approx 1.0587\pi$. Therefore, this CP reads

$$(0.6399\pi)_{1.8442\pi}\pi_{1.0587\pi}(0.6399\pi)_{1.8442\pi}. \tag{2.20}$$

In term of degrees, it reads $115^\circ_{332^\circ}180^\circ_{191^\circ}115^\circ_{332^\circ}$. This composite sequence is related to the well-known sequence SCROFULOUS [38]: $115^\circ_{62^\circ}180^\circ_{281^\circ}115^\circ_{62^\circ}$; the two sequences can be obtained from each other by adding 90° to all phases in our sequence.

2.4.2 *Second-order error correction*

Second-order error compensation is obtained by a composite sequence of at least 4 pulses. A popular CP is the BB1 pulse of Wimperis [37],

$$\text{BB1} = (\pi/2)_0\pi_\chi(2\pi)_{3\chi}\pi_\chi, \tag{2.21}$$

which produces the SU(2) symmetric Splitter gate, with a total pulse area of 4.5π. We have derived a different, asymmetric four-pulse CP,

$$\text{H4a} = \alpha_{\phi_1}\pi_{\phi_2}\pi_{\phi_3}\beta_{\phi_4}, \tag{2.22}$$

where $\alpha = 0.7821\pi$, $\beta = 1.3914\pi$, $\phi_1 = 1.8226\pi$, $\phi_2 = 0.6492\pi$, $\phi_3 = 1.2131\pi$, $\phi_4 = 0.3071\pi$. This pulse has a total area of about 4.17π, i.e. it is faster than the BB1 pulse. It is accurate up to the same order $O(\epsilon^2)$ and produces essentially the same fidelity profile as BB1.

We have also derived a five-pulse composite Hadamard gate by using the symmetric sequence

$$\text{H5s} = \alpha_{\phi_1}\pi_{\phi_2}\pi_{\phi_3}\pi_{\phi_2}\alpha_{\phi_1}, \tag{2.23}$$

with $\alpha = 0.45\pi$, $\phi_1 = 1.9494\pi$, $\phi_2 = 0.5106\pi$, $\phi_3 = 1.3179\pi$. It delivers again the second-order error compensation $O(\epsilon^2)$, however, with a total pulse area of just about 3.9π. Therefore it is considerably faster than the BB1 pulse, by over 13%, while having a similar performance.

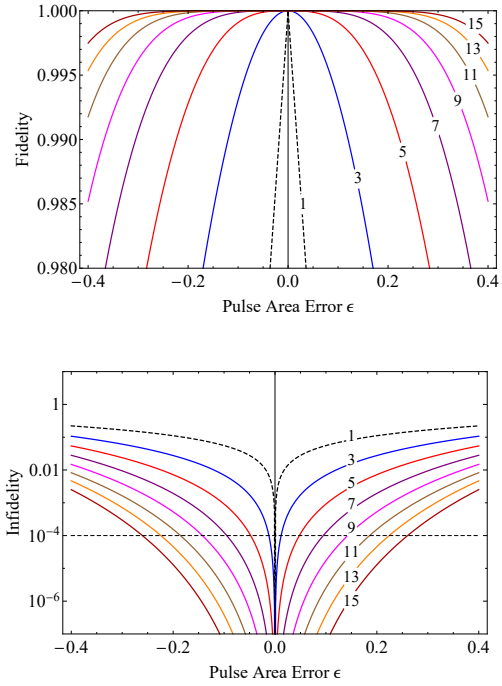

Figure 2.2: Frobenius distance fidelity (top) and infidelity (bottom) of composite Hadamard gates produced by using the symmetric composite sequences H*N*s from Table 2.2 in the main thesis.

2.4.3 *Higher-order error correction*

Similarly to the second order, the *third-order error compensation* is obtained in several different manners, requiring at least 6 pulses. The 6-pulse sequence with the minimal pulse area of about 5.72π reads

$$\mathrm{H6a} = \alpha_{\phi_1}\pi_{\phi_2}\pi_{\phi_3}\pi_{\phi_4}\pi_{\phi_5}\beta_{\phi_6}, \tag{2.24}$$

with $\alpha = 0.5917\pi$, $\beta = 1.1305\pi$, and the phases given in Table 2.2 in the main thesis. The same error correction order is achieved with the symmetric seven-pulse sequence

$$\mathrm{H7s} = \alpha_{\phi_1}\pi_{\phi_2}\pi_{\phi_3}\pi_{\phi_4}\pi_{\phi_3}\pi_{\phi_2}\alpha_{\phi_1}, \tag{2.25}$$

with $\alpha = 0.2769\pi$, and the phases given in Table 2.2 in the main thesis. It produces the same fidelity profile as the 6-pulse sequence but it is a little faster as its pulse area is about 5.55π. Another seven-pulse composite sequence is built similarly to the BB1 sequence (2.21),

$$\mathrm{H7w} = (\pi/2)_{\pi/2}\pi_{\phi_2}\pi_{\phi_3}\pi_{\phi_4}\pi_{\phi_5}\pi_{\phi_6}\pi_{\phi_7}, \tag{2.26}$$

with the phases given in Table 2.2 in the main thesis. It achieves the same error order compensation $O(\epsilon^3)$, however, with a larger total pulse area of 6.5π compared to the previous two CPs.

Fourth-order error compensation is obtained by at least 8 pulses. The 8-pulse sequence with the minimal pulse area of about 7.40π reads

$$\text{H8a} = \alpha_{\phi_1}\pi_{\phi_2}\pi_{\phi_3}\pi_{\phi_4}\pi_{\phi_5}\pi_{\phi_6}\pi_{\phi_7}\beta_{\phi_8}, \tag{2.27}$$

with $\alpha = 0.4954\pi$, $\beta = 0.9028\pi$, and the phases are given in Table 2.2 in the main thesis. The same error correction order is achieved with the symmetric nine-pulse sequence

$$\text{H9s} = \alpha_{\phi_1}\pi_{\phi_2}\pi_{\phi_3}\pi_{\phi_4}\pi_{\phi_5}\pi_{\phi_4}\pi_{\phi_3}\pi_{\phi_2}\alpha_{\phi_1}, \tag{2.28}$$

with $\alpha = 0.2947$, with the phases in Table 2.2 (from the PhD thesis (full text)). Its total pulse area is 7.59π. The BB1-like nine-pulse composite sequence,

$$\text{H9w} = (\pi/2)_{\pi/2}\pi_{\phi_2}\pi_{\phi_3}\pi_{\phi_4}\pi_{\phi_5}\pi_{\phi_6}\pi_{\phi_7}\pi_{\phi_8}\pi_{\phi_9}, \tag{2.29}$$

with the phases in Table 2.2 (from the PhD thesis (full text)), achieves the same fourth-order error compensation $O(\epsilon^4)$, however, with the largest total pulse area of 8.5π compared to the previous two CPs.

The same pattern is repeated for the longer pulse sequences presented in Table 2.2 (from the PhD thesis (full text)): for the same order of pulse area error compensation, the fastest sequences, with the smallest total pulse area are either the asymmetric H*N*a or symmetric H*N*s sequences, and the BB1-like sequences H*N*w are the slowest ones.

The fidelity and the infidelity of the composite Hadamard gates of up to seventh-order error compensation are plotted in Figure 2.2. Obviously, as the number of pulses in the composite sequences, and hence the compensated error order, increase the fidelity and infidelity profiles improve and get broader.

2.5 GENERAL ROTATION GATE

2.5.1 *First-order error correction*

The shortest pulse sequence that can provide a first-order error compensation, as for the X and Hadamard gates, consists of three pulses,

$$\alpha_{\phi_1}\pi_{\phi_2}\alpha_{\phi_1}. \tag{2.30}$$

This composite sequence is related to the SCROFULOUS CP [38], as mentioned above. The values of the pulse area and the composite phases are given in Table 2.3 (from the PhD thesis (full text)).

2.5.2 *More than three pulses*

The five-pulse sequence,

$$\alpha_{\phi_1}\pi_{\phi_2}\pi_{\phi_3}\pi_{\phi_2}\alpha_{\phi_1}, \tag{2.31}$$

provides a second-order error compensation. The sequences with 7, 9, etc. pulses have the same structure and deliver an error compensation of order 3, 4, etc. Generally, a $2n+1$-pulse symmetric sequence of this structure delivers an error compensation up to order $O(\epsilon^n)$. Unfortunately, analytic expressions for the composite parameters for more than three pulses are hard to obtain, if possible at all. Hence we have derived them numerically and their values are listed in Table 2.3 (from the PhD thesis (full text)). The fidelity of these sequences behave similarly to the ones for the X and Hadamard gates.

2.6 COMMENTS AND CONCLUSIONS

In this chapter we presented a number of CP sequences for three basic quantum gates — the X gate, the Hadamard gate and arbitrary rotation gates. The composite sequences contain up to 17 pulses and can compensate up to eight orders of experimental errors in the pulse amplitude and duration. The short composite sequences are calculated analytically and the longer ones numerically.

3

COMPOSITE PULSES FOR ROBUST ULTRAHIGH-FIDELITY PHASE GATES

3.1 INTRODUCTION

Quantum phase gates, such as the Z gate, the S gate and the T gate are key elements in any quantum circuit [100, 102, 103]. An arbitrary phase shift at an angle ϕ, being rotation around z axis, is implemented by at least two resonant π pulses up to an undetectable global phase (see Eq. (1.8)).

The phase gates can be implemented as the sequences of π rotations. Hence, the various quantum control techniques and proposals (see Introduction 2.1 in Chapter 2) that make rotation gates error-resilient, are applicable in this context. Application of CPs to produce well-defined phase shifts of the two states of a qubit is presented in [91]. Here, similarly, we apply CPs to produce composite phase gates [46]. We use analytic approaches and brute-force numerics to derive composite sequences for Z, S, T and general phase gates, which achieve error compensation of up to 8th order. Compensating both major and minor diagonal elements in general phase gate matrix, we also ensure that these CPs are phase-distortionless.

This chapter is organized as follows. In Sec. 3.2 we explain the derivation method. Design and performance of phase gates are presented in Sec. 3.3. Finally, Sec. 3.4 presents the conclusions.

3.2 SU(2) APPROACH

We set zero-error values to the target values,

$$\mathcal{U}_{11}(0) = e^{-i\phi/2}, \quad \mathcal{U}_{12}(0) = 0, \tag{3.1}$$

and we set as many of their derivatives with respect to ϵ, in the increasing order, as possible,

$$\mathcal{U}_{11}^{(m)}(0) = 0, \quad \mathcal{U}_{12}^{(m)}(0) = 0, \quad (m = 1, 2, \ldots, n). \tag{3.2}$$

The largest derivative order n satisfying Eqs. (3.2) gives the order of the error compensation $O(\epsilon^n)$.

3.3 BROADBAND COMPOSITE PHASE GATES

3.3.1 *Design for composite phase gates*

Based on numerical evidence, we consider symmetric type (in pulse areas) of CP sequences, designed by π pulses.

Each symmetric sequence consists of a sequence of $2n+2$ nominal π pulses, with asymmetrically ordered phases,

$$\pi_\nu \pi_{\nu+\phi_1} \pi_{\nu+\phi_2} \cdots \pi_{\nu+\phi_n} \cdot \pi_{\nu+\pi-\frac{1}{2}\phi} \pi_{\nu+\phi_1+\pi-\frac{1}{2}\phi} \pi_{\nu+\phi_2+\pi-\frac{1}{2}\phi} \cdots \pi_{\nu+\phi_n+\pi-\frac{1}{2}\phi}, \tag{3.3}$$

equivalent to

$$\pi_{\nu+\pi+\frac{1}{2}\phi} \pi_{\nu+\phi_1+\pi+\frac{1}{2}\phi} \pi_{\nu+\phi_2+\pi+\frac{1}{2}\phi} \cdots \pi_{\nu+\phi_n+\pi+\frac{1}{2}\phi} \cdot \pi_\nu \pi_{\nu+\phi_1} \pi_{\nu+\phi_2} \cdots \pi_{\nu+\phi_n}. \tag{3.4}$$

From an infinite number of solutions, we choose solutions of the type (3.3) and with a free parameter $\nu = 0$, as the choice of relative phases $\phi_1, \phi_2, \ldots, \phi_n$ is of importance. Henceforth, we target and use a form

$$\pi_0 \pi_{\phi_1} \pi_{\phi_2} \cdots \pi_{\phi_n} \cdot \pi_{\pi-\frac{1}{2}\phi} \pi_{\phi_1+\pi-\frac{1}{2}\phi} \pi_{\phi_2+\pi-\frac{1}{2}\phi} \cdots \pi_{\phi_n+\pi-\frac{1}{2}\phi}, \tag{3.5}$$

and other possible solutions can be obtained by choosing an arbitrary parameter ν in (3.3) or/and by passing to the type (3.4).

3.3.2 *General Phase-shift gate*

As it is well known, such a gate can be produced by two resonant pulses of total temporal area 2π (see (1.8) with $\nu = 0$). The Frobenius distance fidelity (2.7) reads for phase-shift gate $\mathbf{F}(\phi) = \boldsymbol{\mathcal{U}}(0)$

$$\mathcal{F} = 1 - \sqrt{2} \left| \sin \frac{\pi\epsilon}{2} \right| \left| \sin \frac{\phi}{4} \right|. \tag{3.6}$$

For comparison, the trace fidelity is

$$\mathcal{F}_T = 1 - 2 \sin^2 \frac{\pi\epsilon}{2} \sin^2 \frac{\phi}{4}. \tag{3.7}$$

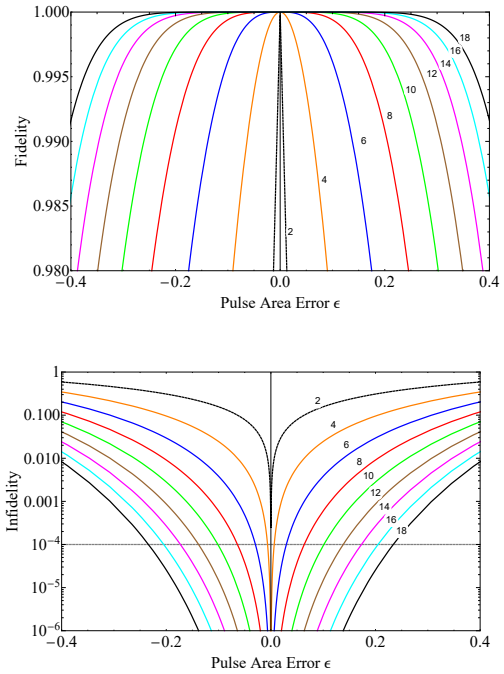

Figure 3.1: Frobenius distance fidelity F (top) and infidelity (bottom) of composite Z gates. The infidelity is in logarithmic scale in order to better visualize the high-fidelity (low-infidelity) range. The numbers N on the curves refer to CP sequences ZN listed in the Table 3.1 in the main thesis.

3.3.2.1 *First-order error compensation*

The careful analysis of Eqs. (3.1) and (3.2) shows that the shortest possible CP which can compensate first-order errors (both in major and minor diagonal elements) consists of four pulses, each with a pulse area of π, and asymmetric phases, with the structure similar to the two pulses,

$$\pi_0 \pi_{\phi_1} \pi_{\pi-\frac{1}{2}\phi} \pi_{\phi_1+\pi-\frac{1}{2}\phi}. \tag{3.8}$$

Solving Eq. (3.1) along with Eq. (3.2) for the first derivatives gives two solutions for the phases,

$$\pi_0 \pi_{-\frac{1}{4}\phi} \pi_{\pi-\frac{1}{2}\phi} \pi_{\frac{3}{4}\pi-\frac{1}{2}\phi}, \tag{3.9a}$$

$$\pi_0 \pi_{\frac{3}{4}\phi} \pi_{\pi-\frac{1}{2}\phi} \pi_{\frac{7}{4}\pi-\frac{1}{2}\phi}. \tag{3.9b}$$

These two sequences generate the same propagator and hence the same fidelity.

Both the Frobenius and the trace distance fidelities depend on the phase flip angle ϕ. The pulse area intervals for the four-pulse composite S4 gates are larger than for the four-pulse composite Z4 gates and smaller than for the four-pulse composite T4 gates. This monotonic pattern persists for longer sequences as well.

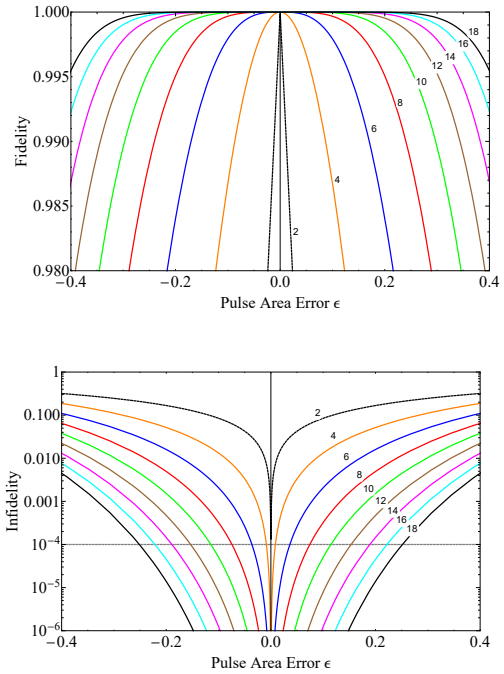

Figure 3.2: Frobenius distance fidelity F (top) and infidelity (bottom) of composite S gates. The infidelity is in logarithmic scale in order to better visualize the high-fidelity (low-infidelity) range. The numbers N on the curves refer to CP sequences SN listed in the Table 3.2 in the main thesis.

3.3.2.2 *Second-order error compensation*

For sequences of six-π pulses, it becomes possible to annul also the second-order derivatives in Eq. (3.2). Design of this asymmetric sequence make it possible to derive analytic solutions

$$\pi_{\phi_0}\pi_{\phi_1}\pi_{\phi_2}\pi_{\phi_0+\pi-\frac{1}{2}\phi}\pi_{\phi_1+\pi-\frac{1}{2}\phi}\pi_{\phi_2+\pi-\frac{1}{2}\phi}, \tag{3.10}$$

The careful analysis of these type of sequences shows that they can be written in a compact form as

$$\pi_{\chi}(2\pi)_0\pi_{\chi+\pi-\frac{1}{2}\phi}(2\pi)_{\pi-\frac{1}{2}\phi}, \tag{3.11a}$$

$$\pi_{\pi+\frac{1}{2}\phi-\chi}(2\pi)_0\pi_{-\chi}(2\pi)_{\pi-\frac{1}{2}\phi}, \tag{3.11b}$$

$$(2\pi)_0\pi_{\pi-\frac{1}{2}\phi+\chi}(2\pi)_{\pi-\frac{1}{2}\phi}\pi_{-\phi+\chi}, \tag{3.11c}$$

$$(2\pi)_0\pi_{-\chi}(2\pi)_{\pi-\frac{1}{2}\phi}\pi_{-\chi+\pi-\frac{1}{2}\phi}, \tag{3.11d}$$

where $\chi = \frac{1}{4}\phi + \arcsin\left(\frac{1}{2}\sin\left(\frac{1}{4}\phi\right)\right)$.

3.3.2.3 *Third-order error compensation*

Nullification of the third-order derivatives in Eq. (3.2) as well, requires eight-π pulses. Here, in contrast to the rotation gates, the composite phase gates with eight pulses

$$\pi_{\phi_0}\pi_{\phi_1}\pi_{\phi_2}\pi_{\phi_3}\pi_{\phi_0+\pi-\frac{1}{2}\phi}\pi_{\phi_1+\pi-\frac{1}{2}\phi}\pi_{\phi_2+\pi-\frac{1}{2}\phi}\pi_{\phi_3+\pi-\frac{1}{2}\phi}, \tag{3.12}$$

can be simplified giving analytic solutions. Careful analysis of these type of sequences shows that they can be written in a compact form as

$$\pi_{\chi}(2\pi)_0\pi_{\chi+\pi-\frac{1}{4}\phi}\pi_{\chi+\pi-\frac{1}{2}\phi}(2\pi)_{\pi-\frac{1}{2}\phi}\pi_{\chi-\frac{3}{4}\phi}, \tag{3.13a}$$

$$\pi_{-\chi+\pi+\frac{1}{4}\phi}(2\pi)_0\pi_{-\chi}\pi_{-\chi-\frac{1}{4}\phi}(2\pi)_{\pi-\frac{1}{2}\phi}\pi_{-\chi+\pi-\frac{1}{2}\phi}, \tag{3.13b}$$

$$(2\pi)_0\pi_{\chi+\pi-\frac{1}{4}\phi}\pi_{\chi+\pi-\frac{1}{2}\phi}(2\pi)_{\pi-\frac{1}{2}\phi}\pi_{\chi-\frac{3}{4}\phi}\pi_{\chi-\phi}, \tag{3.13c}$$

$$(2\pi)_0\pi_{-\chi}\pi_{-\chi-\frac{1}{4}\phi}(2\pi)_{\pi-\frac{1}{2}\phi}\pi_{-\chi+\pi-\frac{1}{2}\phi}\pi_{-\chi+\pi-\frac{3}{4}\phi}, \tag{3.13d}$$

$$\pi_{\chi+\frac{1}{4}\phi}\pi_{\chi}(2\pi)_0\pi_{\chi+\pi-\frac{1}{4}\phi}\pi_{\chi+\pi-\frac{1}{2}\phi}(2\pi)_{\pi-\frac{1}{2}\phi}, \tag{3.13e}$$

$$\pi_{-\chi+\pi+\frac{1}{2}\phi}\pi_{-\chi+\pi+\frac{1}{4}\phi}(2\pi)_0\pi_{-\chi}\pi_{-\chi-\frac{1}{4}\phi}(2\pi)_{\pi-\frac{1}{2}\phi}, \tag{3.13f}$$

where $\chi = \frac{1}{8}\phi + \arcsin\left(\frac{1}{2}\sin\left(\frac{1}{8}\phi\right)\right)$.

3.3.2.4 *Higher-order error compensation*

For CP sequences of more than eight-π pulses, the equations for the composite phases quickly get very bulky and unattainable to guess analytically. General form for these sequences is (3.5).

They reiterate the pattern of the sequences of four, six and eight pulses above: the CP sequences of $2n+2$ pulses have a total pulse area of $(2n+2)\pi$, with all pulses in the sequence being nominal π pulses. Sequences of $2n+2$ pulses produce error compensation of the order $O(\epsilon^n)$ and fidelity profiles

$$\mathcal{F} \cong 1 - \sqrt{2}\left|\sin^{n+1}\frac{\pi\epsilon}{2}\right|\left|\sin\frac{\phi}{4}\right|, \tag{3.14a}$$

$$\mathcal{F}_T \cong 1 - 2\sin^{2n+2}\frac{\pi\epsilon}{2}\sin^2\frac{\phi}{4}, \tag{3.14b}$$

where fidelities are sensitive to the choice of the composite phases and are approximately equal to their precise values.

We have derived numerically the composite phases of this type of sequences of an even number of pulses. They are presented in Tables 3.1, 3.2 and 3.3 in the main thesis

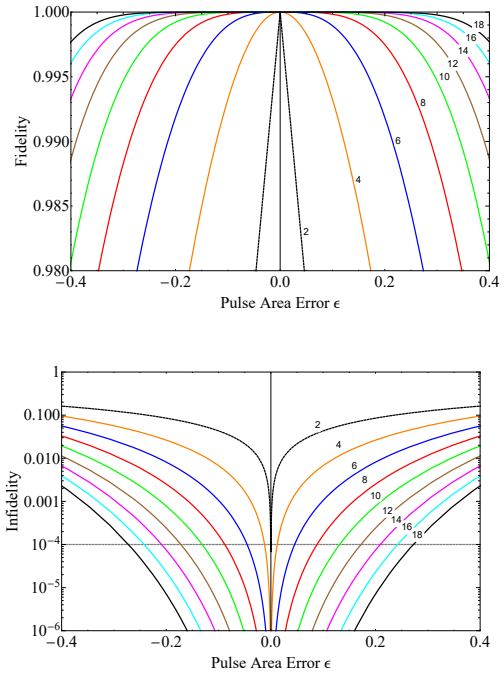

Figure 3.3: Frobenius distance fidelity F (top) and infidelity (bottom) of composite T gates. The infidelity is in logarithmic scale in order to better visualize the high-fidelity (low-infidelity) range. The numbers N on the curves refer to CP sequences TN listed in the Table 3.3 in the main thesis.

for Z, S and T gates correspondingly. The fidelities of these composite Z, S and T gates are plotted in Figures 3.1, 3.2, 3.3 respectively.

It can be seen from the tables and figures that two pulses have very little room for error, since high-fidelity Z, S and T gates allow pulse area errors of less than 0.01%, about 0.01%, about 0.02%, respectively. The four-pulse composite phase gate offers some leeway, with the admissible error of 0.6%, 0.9% and 1.2% for Z, S and T cases. The significant pulse area error correction effect is achieved with the CP sequences of 6 to 10 pulses, for which the high-fidelity range of admissible errors increases from 3% to 10.1% for Z, from 3.6% to 11.5% for S, and from 4.5% to 13.1% for T. Quite notably, errors of up to 23.4%, 25.1% and 27.1% can be eliminated for Z, S and T, and ultrahigh fidelity maintained, with the 18-pulse composite phase gate. Table 3.4 in the main thesis presents composite pulse parameters of general phase gates for different phase angles.

3.4 COMMENTS AND CONCLUSIONS

In this chapter we presented a number of CP sequences for four basic quantum gates — the Z gate, the S gate, the T gate and general phase gates. The CP sequences contain up to 18 pulses and can compensate up to eight orders of experimental errors in the

pulse amplitude and duration. The short CP sequences (up to 8 pulses) are calculated analytically and the longer ones numerically.

Similar class of asymmetric CP sequences for phase gates is derived in [91], where they are build from the θ rotation gates, having twice of total pulse area of them (similar to nesting approach). For this reason, four, eight, twelve, and sixteen CPs are missing, but six, ten, fourteen, and eighteen CPs are given by the simple analytic formula (are more convenient to apply) and have performance equal to the composite gates shown in this chapter. This does not apply to composite phase gates constructed by the universal CPs [77] in [91].

Besides all, the results presented in this chapter can be applied into PO to obtain broadband polarization rotators using stacked single polarization half-wave plates with the optical axes rotated by precisely chosen rotation angles (composite phases). It is able to be done due to quantum-classical analogy of composite rotations on the Bloch and the Poincaré spheres (cf. 6.2). Hereby, we demonstrate the possibility to design the broadband polarization rotators with $\pi/2$, $\pi/4$, $\pi/8$ and arbitrary phase shift angles, by up to 18 CP sequences.

4

NARROWBAND AND PASSBAND COMPOSITE PULSES: APPLICATION TO QUANTUM SENSING

4.1 INTRODUCTION

Although CPs, first, have been used in PO [1, 2], the name, classification and development of the technique belongs to the area of NMR [37, 40, 41, 69, 70, 73, 104, 105]. Being efficient and versatile control technique, CPs may easily adapt to various requirements. This feature manifests in the wide range of applications in both quantum and classical physics — qubit control in trapped ions [11–15, 17, 18], neutral atoms [19], doped solids [20, 21], NV centers in diamond [29, 106], and quantum dots [23–26], high-accuracy optical clocks [30], cold-atom interferometry [31–33], optically dense atomic ensembles [34], magnetometry [35], optomechanics [36], Josephson junctions [107], magnetic resonance imaging (MRI) [108], NMR quantum computation [109], entanglement generation [106], teleportation [11, 110, 111], molecular spectroscopy [112] etc. The possibility of applying a deep neural network for design of CPs is distinguished by its modernity [113].

Constant rotation CPs are independent of the initial state and not permit distortions of the phase of the overall propagator in the rotation axis over a wide error band, if not over the entire error range. Combining in one word, they are "universal" over the entire Bloch sphere, which, for instance, makes them applicable to quantum computation [43]. In NMR and magnetic resonance imaging (MRI), constant rotations are often used in advanced, phase-sensitive (require phase cycling) two-dimensional NMR experiments, like COSY [114] and TOCSY, providing a powerful tool for the determination of the chemical structure of molecules.

This chapter is organized as follows. In Sec. 4.2 we explain the derivation methods. Composite X gates are presented in Sec. 4.3, while composite Hadamard gates in Sec. 4.4. Sec. 4.5 is devoted to the general rotation gates. The last-mentioned three sections are divided into two subsections, presenting narrowband and passband rotations. Finally, Sec. 4.6 presents the conclusions.

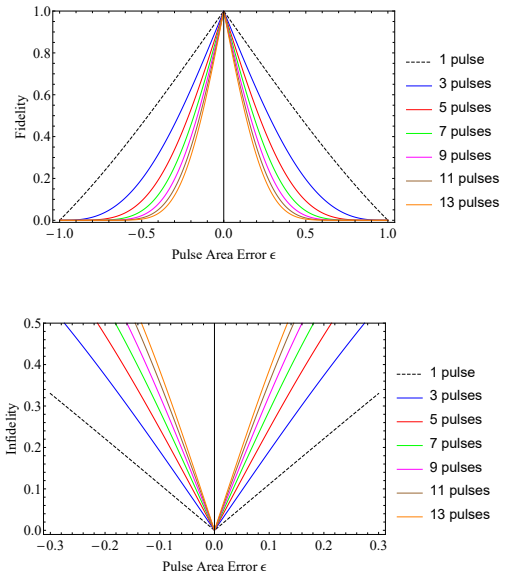

Figure 4.1: Frobenius distance fidelity (top) and infidelity (bottom) of composite X gates produced by the antisymmetric composite sequences AN-m designed by the regularization method from the Table 4.2 in the main thesis.

4.2 DERIVATION

We are dealing with the propagator (1.2) with SU(2) symmetry, where A represents the temporal pulse area $A = \int_{t_i}^{t_f} \Omega(t)\,\mathrm{d}t$ in quantum optics, the pulse width or amplitude θ in NMR, and the phase shift $\varphi = 2\pi L(n_f - n_s)/\lambda$ [115] in PO. Without loss of generality of the problem, we will use the terminology of QC.

4.2.1 *Narrowband composite pulses*

4.2.1.1 *SU(2) approach*

Here, we set as many of their derivatives with respect to ϵ at ± 1, in the increasing order, as possible,

$$\mathcal{U}_{11}^{(m)}(\pm) = 0, \quad \mathcal{U}_{12}^{(m)}(\pm) = 0, \quad (m = 1, 2, \ldots, n_s). \tag{4.1}$$

Derivation of the NB CPs requires the solution of Eqs. (2.4) and (4.1). We do this numerically by using standard routines in MATHEMATICA: we minimize the following loss or error function of optimization

$$\mathcal{E} = \mathcal{E}_0 + \sum_{k=1}^{n_s} \left[|\mathcal{U}_{11}^{(k)}(-)|^2 + |\mathcal{U}_{11}^{(k)}(+)|^2 + |\mathcal{U}_{12}^{(k)}(-)|^2 + |\mathcal{U}_{12}^{(k)}(+)|^2 \right], \tag{4.2}$$

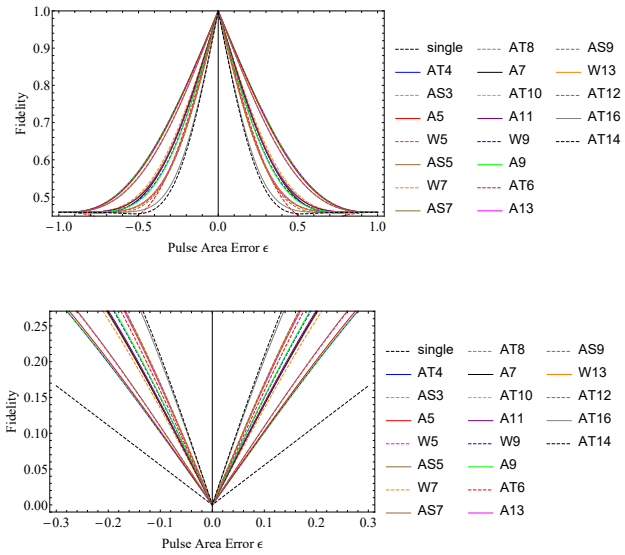

Figure 4.2: Frobenius distance fidelity (top) and infidelity (bottom) of composite narrowband Hadamard gates produced by the four families of composite sequences from the Table 4.3 in the main thesis.

where the initial condition (targeted gate) is captured by $\mathcal{E}_0 = |\mathcal{U}_{11}(0) - \cos\theta/2|^2 + |\mathcal{U}_{12}(0) - \sin\theta/2|^2$, and n_s is the narrowness or sensitivity order.

4.2.1.2 *Modified-SU(2) approach*

Major and minor diagonal elements of SU(2) matrix are related $|\mathcal{U}_{11}(\epsilon)|^2 + |\mathcal{U}_{21}(\epsilon)|^2 = 1$, being Cayley-Klein parameters. Due to this dependence, optimization of one will directly narrower the other one. To ensure the stability of the phase of constant rotation, we optimize the minor diagonal element. So, the loss function is the following

$$\mathcal{E} = \mathcal{E}_0 + \sum_{k=1}^{2n_s} \Big[|\mathcal{U}_{12}^{(k)}(-)|^2 + |\mathcal{U}_{12}^{(k)}(+)|^2 \Big]. \tag{4.3}$$

Modified SU(2) approach works for X gate or π rotations, and give better results than by using SU(2). The number of derivatives optimized by both methods is equal, but by this method the minor element (of the actual gate matrix) $\mathcal{U}_{21}(\epsilon)$ is optimized by the order of $2n_s$, two times the sensitivity order.

4.2.2 *Passband composite pulses*

4.2.2.1 *SU(2) approach*

As already mentioned, PB CPs have the properties of both BB and NB CPs. In addition to the narrowband property (4.1), we add broadband property

$$\mathcal{U}_{11}^{(k)}(0) = 0, \quad \mathcal{U}_{12}^{(k)}(0) = 0, \quad (k = 1, 2, \ldots, n_r), \tag{4.4a}$$

$$\mathcal{U}_{11}^{(m)}(\pm) = 0, \quad \mathcal{U}_{12}^{(m)}(\pm) = 0, \quad (m = 1, 2, \ldots, n_s). \tag{4.4b}$$

Now, in addition to sensitivity order n_s in Eq. (4.4b), we also have n_r which is the largest derivative order satisfying Eq. (4.4a) and gives the order of robustness $O(\epsilon^{n_r})$. Pulse sequence with any combination of n_s and n_r both greater than one is passband. Therefore, we examine two types of passband CPs, namely

- *pari passu* passband CPs, for which robustness and sensitivity orders are equal and define the passband order $n_p = n_r = n_s$,
- *diversis passuum* passband CPs, for which one of the above properties is superior to the other $n_r \neq n_s$.

Derivation of the PB CPs requires the solution of Eqs. (2.4), and (4.4). We do this numerically by using standard routines in MATHEMATICA: we minimize the following loss function of optimization

$$\begin{aligned}\mathcal{E} = \mathcal{E}_0 &+ \sum_{k=1}^{n_r}\left[|\mathcal{U}_{11}^{(k)}(0)|^2 + |\mathcal{U}_{12}^{(k)}(0)|^2\right] + \\ &+ \sum_{k=1}^{n_s}\left[|\mathcal{U}_{11}^{(k)}(-)|^2 + |\mathcal{U}_{11}^{(k)}(+)|^2 + |\mathcal{U}_{12}^{(k)}(-)|^2 + |\mathcal{U}_{12}^{(k)}(+)|^2\right].\end{aligned} \tag{4.5}$$

4.2.2.2 *Regularization approach*

Results obtained by the SU(2) method of derivation besides SK1 and PB1, had wiggles on the edges, arising negative fidelity. The optimization method, alternative to SU(2), is more flexible and gives better results is a regularization method

$$\begin{aligned}\mathcal{E} = \mathcal{E}_0 &+ \sum_{k=1}^{2n_p}\left[|\mathcal{F}_{\mathrm{T}}^{(k)}(0)|^2 + |\mathcal{F}_{\mathrm{T}}^{(k)}(-)|^2 + |\mathcal{F}_{\mathrm{T}}^{(k)}(+)|^2\right] + \\ &+ \lambda\Big[|\mathcal{U}'_{11}(0)|^2 + |\mathcal{U}'_{12}(0)|^2 + |\mathcal{U}'_{11}(+)|^2 + \\ &+ |\mathcal{U}'_{11}(-)|^2 + |\mathcal{U}'_{12}(+) + |\mathcal{U}'_{12}(-)|^2\Big],\end{aligned} \tag{4.6}$$

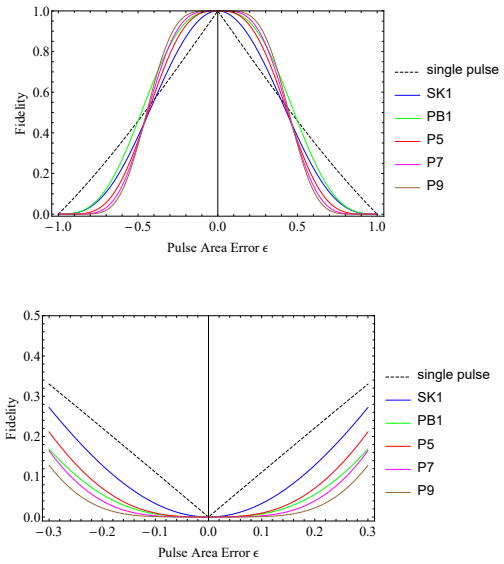

Figure 4.3: Frobenius distance fidelity (top) and infidelity (bottom) of composite passband X gates produced by PN (pari passu) sequences from the Table 4.4 in the main thesis.

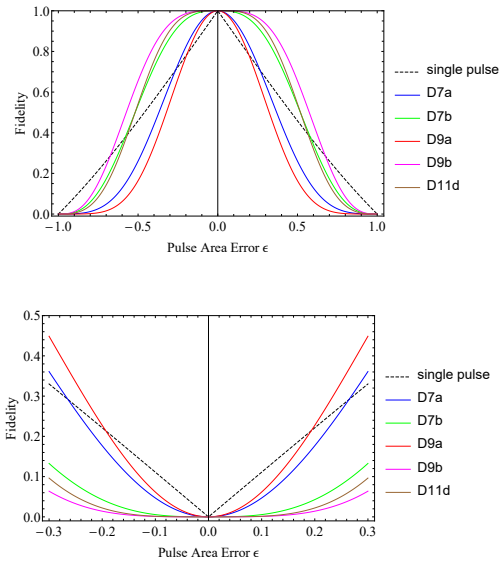

Figure 4.4: Frobenius distance fidelity (top) and infidelity (bottom) of composite passband X gates produced by DN (diversis passuum) sequences from the Table 4.6 in the main thesis.

where $2n_p$ orders of narrowness/broadness of trace fidelity of SU(2) matrix are optimized, which is equivalent to the optimization of SU(2) matrix elements by the order of n_p (two times lower). A regularizer $\lambda \neq 0$ constrains the result to be constant rotation and without unnecessary wiggles. In our optimization, it is taken $\lambda = 1$.

4.2.3 *Performance measures*

Since we consider constant rotations, the fidelities can not be negative, while it can be the case for CPs alternating at the bottom, i.e. like NB2 and PB2. Since we do not have alternations or wiggles of the fidelity and the minimum of fidelity is at it's boundaries $\epsilon = \pm 1$ and depends on the θ parameter

$$[\mathcal{F}_T(\theta)]_{min} = [\mathcal{F}_T(\theta)]_{\epsilon=\pm 1} = \cos\frac{\theta}{2}, \tag{4.7a}$$

$$[\mathcal{F}(\theta)]_{min} = [\mathcal{F}(\theta)]_{\epsilon=\pm 1} = 1 - \sqrt{1 - \cos\frac{\theta}{2}}. \tag{4.7b}$$

We propose to use the measure $\Delta(\alpha_0) = |\epsilon(\mathcal{F} = \alpha_0)| - |\epsilon(\mathcal{F} = 1 - \alpha_0)|$ of the rectangularity of passband CPs. In our case for rotation gates, we choose α_0 equal to 10^{-4}, which corresponds to the quantum computation benchmark, and rectangularity measure $\Delta \triangleq \Delta(10^{-4})$ is the difference between absolute errors at UL-(ultralow) and UH-fidelities (ultrahigh). Since the slope coefficient (is approximated by a straight line $\tan\beta_0 \simeq \frac{\Delta\mathcal{F}}{\Delta(\alpha_0)} = \frac{1-2\alpha_0}{\Delta(\alpha_0)}$) is inversely proportional to Δ, hence, smaller Δ, higher the rectangularity of the fidelity line.

4.3 X GATE

4.3.1 *Narrowband*

We set two appropriate designs of CPs — antisymmetric AN and Wimperis-kind WN, both are the sequences of π pulses.

If we target pure π composite rotations ($\phi = 0$), AN has the following structure or design

$$\pi_{\phi_1}\pi_{\phi_2}\cdots\pi_{\phi_{n_s}}\pi_{\phi_{n_s+1}}\pi_{-\phi_{n_s}}\cdots\pi_{-\phi_2}\pi_{-\phi_1}, \tag{4.8}$$

and consists of the odd number of π pulses, which besides the middle one, have phases with equal absolute value but with opposite signs when tracking from the left to right and from the right to left. Since we target X gate ($\phi = \pi/2$), $\pi/2$ is added to all phases with both minus and plus signs $\pm\phi_k \to \pm\phi_k + \pi/2$.

Again, for π composite rotations ($\phi = 0$), WN design looks more interpretable

$$\pi_{\phi_1}\pi_{\phi_2}\pi_{\phi_3}\cdots\pi_{\phi_{n_s+1}}\pi_{\phi_{n_s+1}}\cdots\pi_{\phi_3}\pi_{\phi_2}, \tag{4.9}$$

and consists of the odd number of π pulses, where, besides the first pulse, the second half of the structure is a mirror image of the first half, i.e. in the second half, phases

are written in the opposite direction. Again, since we target X gate ($\phi = \pi/2$), $\pi/2$ is added to all phases $\phi_k \to \phi_k + \pi/2$.

Lowest member of WN is the well-known NB1 pulse of Wimperis (W5), hence the name of the design. AN and WN CPs for X gate derived by SU(2) approach are listed in Table 4.1 in the main thesis. Curiously, for X gate or π rotation, the modified-SU(2) approach improves the results obtained by the SU(2) method. We derived up to 13 CPs by this method, called AN-m, which have the same antisymmetric design of AN.

4.3.2 *Passband*

4.3.2.1 *Pari passu*

Difficulty of derivation of the passband rotation gates is manifested in the appearance of alternation in fidelity (deriving by SU(2)), not established by the derivation method, exhibiting their tenderness. This problem can be solved by using a regularization method, instead of the strict SU(2) method. Despite that it was possible to derive SK1 and PB1 as the first and second order pari passu passband pulses, respectively (wiggles arise for longer sequences). In both methods, the design of pari passu passband pulses is the same

$$\pi_{\phi_1}(2\pi)_{\phi_2}(2\pi)_{\phi_3}\cdots(2\pi)_{\phi_N}. \tag{4.10}$$

Sequences obtained by regularization method PN for X gate are listed in Table 4.4 in the main thesis. Increasing the number of pulses, performance measures, namely, sensitivity, robustness and rectangularity, improve regularly.

4.3.2.2 *Diversis passuum*

Heterogeneous optimization of broadband and narrowband properties generates another type of passband pulses, called diversis passuum, which can be derived using SU(2) method, denoted as DN

$$\pi_{\phi_1}\pi_{\phi_2}\cdots\pi_{\phi_N}, \tag{4.11}$$

which don't have special design in general, although for the lowest members D7a and D7b phases have a simple structure (see Table 4.6 in the main thesis).

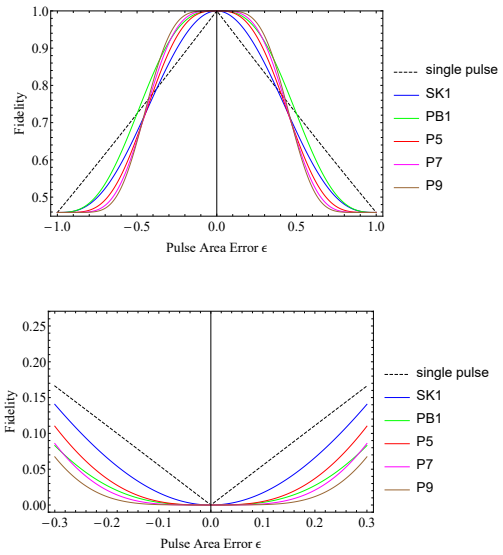

Figure 4.5: Frobenius distance fidelity (top) and infidelity (bottom) of composite passband Hadamard gates produced by P*N* (pari passu) sequences from the Table 4.5 in the main thesis.

4.4 HADAMARD GATE

4.4.1 *Narrowband*

For optimization of non-π rotations, the SU(2) method is used. Four designs or structures can be used to derive narrowband Hadamard gate — antisymmetric 1st type and 2nd type, Wimperis-kind and asymmetric, general structure of which liberally presented in Sec. 4.5.1. Corresponding members of these four families are displayed in Table 4.3 in the main thesis and Fig. 4.2.

4.4.2 *Passband*

Pari passu passband P*N* CPs for Hadamard gate have the structure presented in Sec. 4.5.2 and are displayed in Table 4.5 in the main thesis.

Diversis passuum passband D*N* CPs for Hadamard gate have the structure presented in Sec. 4.5.2 and are displayed in Table 4.7 in the main thesis.

4.5 GENERAL ROTATION GATE

4.5.1 *Narrowband*

Generalization of AN CPs, i.e. antisymmetric sequencese of 1st type, have the following structure in general presented by θ parameter

$$\left(\frac{\pi-\theta}{2}\right)_{\phi_0}\pi_{\phi_1}\cdots\pi_{\phi_{n_s}}\pi_{\phi_{n_s+1}}\pi_{-\phi_{n_s}}\cdots\pi_{-\phi_1}\left(\frac{\pi-\theta}{2}\right)_{-\phi_0}. \tag{4.12}$$

When targeting general rotation gates ($\phi = \pi/2$), as usual, this $\pi/2$ phase change must be done for all the components in the structure. For non-π rotations the number of pulses is $N = 2n_s + 3$, where n_s is the sensitivity order. In the case of π rotations ($\theta = \pi$) we transition to the Eq. (4.8), where one gets rid of the first and the last pulses (being zero rotations), hence ϕ_0, and the number of constituent pulses becomes $N = 2n_s + 1$. General formula for the number of pulses and total operation time can be presented using a step function σ,

$$N(\theta) = 2n_s + 1 + 2\sigma(\theta), \tag{4.13a}$$

$$\mathcal{A}_{tot}(\theta) = N(\theta)\pi - 2\theta, \tag{4.13b}$$

$$\sigma(\theta) = \begin{cases} 1 & \text{if } \theta \in (0,\pi), \\ 0 & \text{if } \theta = \pi. \end{cases} \tag{4.13c}$$

Alternatively, one may use 2nd type of antisymmetric design ATN

$$\alpha_{\phi_1}\pi_{\phi_2}\cdots\pi_{\phi_{n_s+1}}\pi_{-\phi_{n_s+1}}\cdots\pi_{-\phi_2}\alpha_{-\phi_1}, \tag{4.14}$$

where the all phase structure is added by $\pi/2$ to obtain a general rotation gate.

Two asymmetric sequences are also useful for general rotation gates, Wimperis-kind and just asymmetric. Wimperis-kind WN design, written for $\phi = 0$, is

$$\theta_{\phi_1}\pi_{\phi_2}\cdots\pi_{\phi_{2n_s+1}}. \tag{4.15}$$

Since the sequence of π pulses in the CP carry the optimization process and seeds a stable design, the most fictitious asymmetric pulse may have the following design

$$\alpha_{\phi_1}\pi_{\phi_2}\pi_{\phi_3}\cdots\pi_{\phi_{2n_s-1}}\pi_{\phi_{2n_s}}\beta_{\phi_{2n_s+1}}, \tag{4.16}$$

denoted as ASN. Sometimes, it is possible to find the best trade-off in speed and accuracy by these sequences. Good example is AS9 in Table 4.3 in the main thesis.

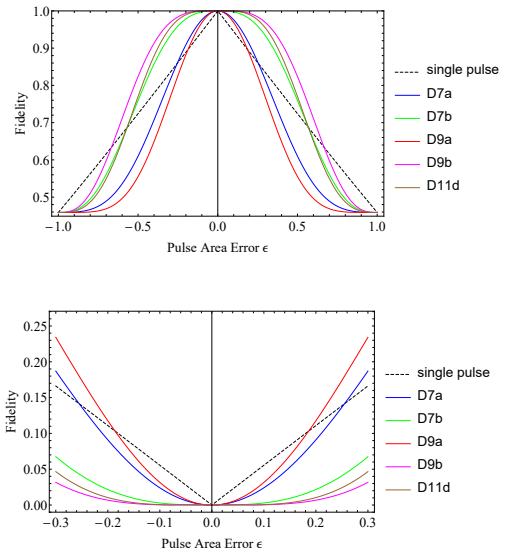

Figure 4.6: Frobenius distance fidelity (top) and infidelity (bottom) of composite passband Hadamard gates produced by DN (diversis passuum) sequences from the Table 4.7 in the main thesis.

4.5.2 *Passband*

Pari passu passband rotation gates PN are subjected to the following design ($\phi = \pi/2$ must be added to all the phases)

$$\theta_{\phi_1}(2\pi)_{\phi_2}(2\pi)_{\phi_3}\cdots(2\pi)_{\phi_{2np+1}}, \tag{4.17}$$

which can be considered as the generalization of the SK1:

$$\theta_0(2\pi)_{\chi}(2\pi)_{-\chi}, \tag{4.18}$$

where $\chi = \arccos\left(-\frac{\theta}{4\pi}\right)$, and the PB1:

$$\theta_0(2\pi)_{\chi}(2\pi)_{-\chi}(2\pi)_{-\chi}(2\pi)_{\chi}, \tag{4.19}$$

where $\chi = \arccos\left(-\frac{\theta}{8\pi}\right)$.

Diversis passuum passband rotation gates DN have the design similar to (4.15)

$$\theta_{\phi_1}\pi_{\phi_2}\cdots\pi_{\phi_{2(n_r+n_s)+1}}, \tag{4.20}$$

but here the number of pulses is equal to $N = 2(n_r + n_s) + 1$.

4.6 CONCLUSIONS

We presented CPs which produce narrowband and passband rotational single-qubit gates, namely — X, Hadamard and general rotation gates.

Three types of optimization methods were used — SU(2), modified-SU(2), and regularization. The antisymmetric A5-m pulse outperforms well-known NB1 — FWHM of A5-m is about 42.8%, which is narrower than FWHM of NB1 49.4% of whole error bandwidth.

We propose two types of passband CPs — *pari passu* PN, with passband order, and *diversis passuum* DN, with different sensitivity and robustness orders.

The results in this chapter can be useful in applications such as spatial localization in *in vivo* NMR spectroscopy, selective and local spatial addressing of trapped ions or atoms in optical lattices by tightly focused laser beams in QS, narrowband polarization filters and passband polarization retarders in PO.

5

COMPOSITE SEQUENCES FOR ULTRASMALL TRANSITION PROBABILITY: APPLICATION TO DETERMINISTIC SINGLE-PHOTON EMISSION

In some applications of quantum control, it is necessary to produce very weak excitation of a quantum system. Such an example is presented by the concept of single-photon generation in cold atomic ensembles or doped solids, e.g. by the DLCZ protocol, for which a single excitation is shared among thousands and millions atoms or ions. Another example is the possibility to create huge Dicke state of N qubits sharing a single or a few excitations. Other examples are using tiny rotations to tune high-fidelity quantum gates or using these tiny rotations for testing high-fidelity quantum process tomography protocols. Ultrasmall excitation of a quantum transition can be generated by either a very weak or far-detuned driving field. However, these two approaches are sensitive to variations in the experimental parameters, e.g. the transition probability varies with the square of the pulse area. Here we propose a different method for generating a well-defined pre-selected very small transition probability — of the order of 10^{-2} to 10^{-8} — by using composite pulse sequences. The method features high fidelity and robustness to variations in the pulse area and the pulse duration.

5.1 INTRODUCTION

In almost all applications of quantum control, the focus is either on complete population inversion (known as X gate in quantum information) or half excitation (known as Hadamard or $\sqrt{X}$ gate in quantum information). These are produced most often by resonant excitation by π and $\pi/2$ pulses, but adiabatic and composite methods have also been used. These methods have different advantages and shortcomings. For instance, resonant excitation is the fastest method and is very accurate if the parameter values are very precise [116, 117], but it is sensitive to parameter variations. Adiabatic

methods [49, 59] are robust to experimental errors but are slow and it is difficult to reach high accuracy with them. (A cure is offered by the "shortcuts-to-adiabaticity" approach [118], but it comes with the necessity of accurate pulse shaping or additional fields.) Composite pulses — trains of pulses with well-defined relative phases used as control parameters [40, 41] — sit somewhere in the "sweet spot" as they feature extreme accuracy and robustness, while being significantly faster than adiabatic methods (but slower than resonant excitation by a factor of 2-3 or more).

However, quantum control offers the opportunity for partial excitation with any transition probability, rather than just 1 and $\frac{1}{2}$. For instance, there are applications in which a very small transition probability is required. One prominent example is the DLCZ protocol for single-photon generation in an ensemble of ultracold atoms or in a doped solid and its variations and extensions [119–125]. Single photons are the physical platform for such advanced technologies as quantum communications [126–130] and photonic quantum computing [131–134]. In this protocol, a three-level Raman system $|g_1\rangle \leftrightarrow |e\rangle \leftrightarrow |g_2\rangle$ is used. In the *writing* process, the atomic transition $|g_1\rangle \leftrightarrow |e\rangle$ is excited with a very low probability by an off-resonant laser pulse with a wave vector $\overrightarrow{k_w}$, such that a single (or a few) atomic excitation is stored in the ensemble as a shared excitation by all atoms. Then collective spontaneous emission on the transition $|e\rangle \rightarrow |g_2\rangle$ occurs at a random time, in which a (Stokes) photon is emitted in a random direction. However, a single-photon detector is placed along a particular spatial direction and any click in it is considered as a "heralded" photon, with a well-defined wave vector $\overrightarrow{k_s}$. In the *reading* process, a resonant laser pulse with a wave vector $\overrightarrow{k_r}$ is applied on the atomic transition $|g_2\rangle \leftrightarrow |e\rangle$, which stimulates the emission of a (anti-Stokes) photon on the pump transition $|e\rangle \rightarrow |g_1\rangle$, in a well-defined spatial direction $\overrightarrow{k_a}$, determined by the phase-matching condition $\overrightarrow{k_a} = \overrightarrow{k_s} + \overrightarrow{k_w} - \overrightarrow{k_r}$. In this protocol, one of the crucial conditions is to be able to produce only one shared excitation among a large number of atoms N, i.e. a driving field which generates a transition probability of $1/N$ is needed.

Another example is the possibility to create huge entangled Dicke states [135]. These very special states share a fixed number of excitations n evenly among N qubits, a special case of which (for $n = 1$) is the W state. A prominent feature of the Dicke states is that they are immune against collective dephasing, which is ubiquitous in various systems. Therefore, the Dicke sub-space, which is $N!/n!(N-n)!$-dimensional, can be used as a decoherence-free computational subspace [136–138]. Dicke states possess genuine multi-partite entanglement [139, 140], which is, moreover, very robust against particle loss [141–143]: the loss of a qubit reduces the N-dimensional Dicke state to a $N-1$-dimensional one. Dicke states have been proposed and demonstrated in various physical systems, including ensembles of neutral atoms [144, 145], trapped ions [146–149], quantum dots [150], and using linear optics [145, 151]. Many of these proposals

and demonstrations have various restrictions, as they cannot create arbitrary but only particular Dicke states, individual qubit addressing is required, the number of the necessary physical interactions scales very fast with N, a special initial (Fock) state is required, insufficient efficiency, very long interaction times, etc. Composite pulses of ultrasmall probability offer a direct path toward the creation of large Dicke states as they can produce a specific number of shared excitations among large-N ensembles of qubits.

A third example when a well-defined small transition probability is needed arises when fine tuning quantum gates: in order to reach ultrahigh gate fidelity a rotation gate at a well-defined tiny angle can be very useful. Moreover, such small rotations alone can be used to test the accuracy of various quantum process tomography protocols.

In this paper, we address this specific problem by designing composite pulse sequences, which seem to be the only quantum control technique capable to generate a tiny transition probability that is robust to variations of the experimental parameters. The dominant majority of composite pulses in the literature are designed to produce specific rotations on the Bloch sphere, typically at angles π (generating complete population transfer), $\pi/2$ (half population transfer), $\pi/4$ and $3\pi/4$, as reviewed in Refs. [40, 41]. There exist just a few composite sequences which produce general rotations at arbitrary angles [37, 43, 73, 74, 83, 152]. Some of them can be used for the present task of ultrasmall probability and they are listed below, along with many newly derived composite sequences.

Composite rotations are broadly divided into two large groups called variable and constant rotations. The variable rotations [40, 83, 152] feature well-defined transition probability but not well-defined phases of the propagator. Constant (or phase-distortionless rotations) feature both well-defined populations and well-defined phases of the propagator [37, 73, 74]. There are large markets for either of these, with only constant rotations being suitable for quantum gates. However, they are much more demanding to generate and much longer than variable rotations, for the same order of error compensation. This will be clearly seen below as we consider one type of constant rotations and two types of variable rotations.

After a description of the derivation method we present specific composite sequences of 2, 3 and 4 pulses, many of which have analytic expressions for the composite parameters, and then proceed to longer sequences.

5.2 THE METHOD

We wish to construct composite pulses, which produce a very low probability of transition between two states $|1\rangle \rightarrow |2\rangle$, in an efficient and robust manner. Such composite

pulses are known as θ-pulses, as they produce a transition probability $p = \sin^2(\theta/2)$. In the NMR literature one can find a number of θ pulses for $\theta = \pi/4$ (called 45° pulses), $\theta = \pi/2$ (called 90° pulses), and $\theta = 3\pi/4$ (called 135° pulses). Very few general formulae for an arbitrary value of θ exist in the literature. In our case we need composite pulses, which produce transition probability $p = 1/N \ll 1$, which implies $\theta \ll 1$. Such composite pulses are designed here.

Each pulse in a composite sequence is considered resonant and hence it generates the propagator

$$\mathbf{U}(A,\phi) = \begin{bmatrix} \cos(A/2) & -ie^{i\phi}\sin(A/2) \\ -ie^{-i\phi}\sin(A/2) & \cos(A/2) \end{bmatrix}, \tag{5.1}$$

where ϕ is the phase of the coupling. The overall propagator for a sequence of n pulses,

$$(A_1)_{\phi_1}(A_2)_{\phi_2}\cdots(A_n)_{\phi_n}, \tag{5.2}$$

each with a pulse area A_k and phase ϕ_k, reads

$$\mathbf{U}_n = \mathbf{U}(A_n,\phi_n)\mathbf{U}(A_{n-1},\phi_{n-1})\cdots\mathbf{U}(A_2,\phi_2)\mathbf{U}(A_1,\phi_1), \tag{5.3}$$

which, by convention, acts from right to left. One of the phases is always irrelevant for the physically observed quantities (it is related to the global phase of the wavefunction), and can be set to zero. As such, we always choose the first phase: $\phi_1 = 0$. In other words, all other phases are relative phases of the respective pulse to the phase of the first pulse.

The pulse areas A_k and the phases ϕ_k are the control parameters, which are selected from the conditions that the transition probability,

$$P = |\mathbf{U}_{12}|^2, \tag{5.4}$$

has a specific target value p and it is robust to variations ϵ in the pulse area $A_k(1+\epsilon)$. The error-free values of the pulse areas A_k are called *nominal* values. The relative error ϵ is assumed to be the same for all pulses in the composite sequence. This is reasonable if they are derived from the same source, which is usually the case.

The multiplication of the two-dimensional matrices in Eq. (5.3) leads to rapidly growing expressions. Still, these are far more manageable than the ones coming from the three-dimensional matrices in the usual Bloch-vector derivation of composite sequences.

One can proceed in two directions.

- One possibility is to expand the transition probability of Eq. (5.4) in a Taylor-Maclaurin series vs ϵ. The coefficients in this series are functions of all A_k and ϕ_k ($k = 1, 2, \ldots, n$). We nullify as many of the first few such coefficients (i.e. derivatives vs ϵ) as possible, which generate a set of equations for A_k and ϕ_k. The result is a transition probability with a Taylor-Maclaurin series expansion

$$P(\epsilon) = p + O(\epsilon^m), \tag{5.5}$$

  where p is the target value. We say that the respective composite sequence is accurate up to order $O(\epsilon^m)$. We shall first present such composite sequences, which are known as *variable rotations* in NMR and allow to easily reach error compensation of very high order.

- Alternatively, one can take the propagator elements $U_{11} = U_{22}^*$ and $U_{12} = -U_{21}^*$, expand them in Taylor-Maclaurin series vs ϵ, and carry out elimination of as many lowest-order terms as possible. The result is a Taylor-Maclaurin expansion of the propagator,

$$\mathbf{U}_n(\epsilon) = \mathbf{U}_n + O(\epsilon^l). \tag{5.6}$$

  Obviously, with the same number of free parameters, one can cancel of factor of 2 fewer terms now, than in the expansion of the probability P. However, the resulting composite sequences will be stabilized with respect to both the amplitudes and the phases of the overall propagator, rather than with respect to the amplitudes only, as with Eq. (5.5). Such composite sequences create constant rotations in NMR language, or, in quantum information terms, *quantum rotation gates*.

We begin with the first approach, which delivers expressions as in Eq. (5.5), and then proceed with the second approach, which delivers expressions of the type (5.6).

5.3 SMALL-PROBABILITY COMPOSITE SEQUENCES

5.3.1 *Two-pulse composite sequences*

We have derived two types of two-pulse composite sequences.

5.3.1.1 *Symmetric sequence of pulses*

In the first type, the two pulse areas are equal to $\pi/2$,

$$S2: \quad (\tfrac{1}{2}\pi)_0(\tfrac{1}{2}\pi)_{\pi-\theta}. \tag{5.7}$$

The transition probability is

$$P = \cos^2\frac{\pi\epsilon}{2}\sin^2\frac{\theta}{2}. \tag{5.8}$$

For

$$\theta = \arccos(1-2p) = 2\arcsin(\sqrt{p}), \tag{5.9}$$

we find

$$P = p[1-\sin^2(\frac{1}{2}\pi\epsilon)] = p[1+O(\epsilon^2)]. \tag{5.10}$$

This simplest composite sequence is accurate up to the second order $O(\epsilon^2)$. For example, for probabilities $p = 10^{-2}$, 10^{-3}, 10^{-4} and 10^{-5} we find $\phi = 0.0638\pi$, 0.0201π, 0.0064π, and 0.0020π. These values correspond to 11.48°, 3.62°, 1.15°, and 0.36°.

The advantage of these sequences is their extreme simplicity and the analytic formula for the phase, which make it possible to immediately write down the sequence for any target transition probability. The disadvantage is the availability of a single control parameter only, which limits the error compensation to the first order only. This is still superior over a single resonant pulse, which is accurate to zeroth order only.

5.3.1.2 *Asymmetric sequence of pulses*

In the second two-pulse sequence, the pulse areas are different,

$$A2: \quad (A_1)_0(A_2)_{\phi_2}. \tag{5.11}$$

Here we have three control parameters — two pulse areas and a phase — which allow us to compensate higher orders of errors. Now closed analytic expressions for the parameters are not possible to derive. However, due to the fact that $p \ll 1$, we can use perturbation theory, which gives us the approximations

$$A_1 = x - y, \quad A_2 = x + y, \quad \phi_2 = \pi - \phi, \tag{5.12}$$

with $x \approx 0.7151\pi$, $y \approx 0.2553\pi\sqrt{p}$, and $\phi \approx 0.4875\pi\sqrt{p}$. All these are valid for $p \ll 1$. The pulse areas and the phases for a few values of the transition probability are given in Table 5.1.

The advantage of the composite sequence (5.11) over the symmetric one (5.7) is that it is accurate to the third order in ϵ,

$$P = p[1+O(\epsilon^3)]. \tag{5.13}$$

The disadvantage is that it requires a larger total pulse area, about 1.43π compared to just π for the symmetric sequence (5.7).

p	A_1	A_2	ϕ
10^{-2}	0.689806	0.741105	0.048767
10^{-3}	0.707103	0.723255	0.015417
10^{-4}	0.712599	0.717704	0.004875
10^{-5}	0.714341	0.715956	0.001542
10^{-6}	0.714894	0.715404	4.88×10^{-4}
10^{-7}	0.715068	0.715229	1.54×10^{-4}
10^{-8}	0.715123	0.715174	4.88×10^{-5}

Table 5.1: Pulse areas and phases (in units of π) for the composite sequence (5.11) (in units of π) for a few values of the transition probability. All composite sequences have the error order $O(\epsilon^3)$.

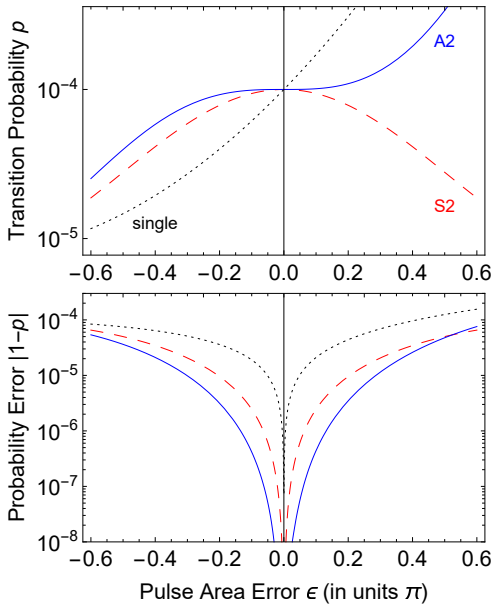

Figure 5.1: Performance of the two-pulse composite sequences (5.7) (red dashed) and (5.11) (blue solid) for the transition probability $p = 10^{-4}$. The dotted curves show the single pulse excitation probability for comparison.

The performance of the two sequences is compared in Fig. 5.1. Both sequences (5.7) and (5.11) outperform significantly the conventional single-pulse excitation probability, which is very sensitive to pulse area errors. The asymmetric sequence A2 of Eq. (5.11), with its three control parameters and error order $O(\epsilon^3)$, outperforms the symmetric sequence S2 of Eq. (5.7), which has only one control parameter and error order $O(\epsilon^2)$.

5.3.2 *Three-pulse composite sequences*

We have derived three three-pulse composite sequences, two symmetric and one asymmetric.

5.3.2.1 *Symmetric sequence of pulses*

The symmetric sequence of pulses reads

$$S3: \quad (\tfrac{1}{2}\pi)_0 \pi_{\alpha+\beta} (\tfrac{1}{2}\pi)_{2\beta}, \tag{5.14}$$

where

$$\alpha = \theta/2, \tag{5.15a}$$
$$\beta = \arccos(\sin\alpha - \cos\alpha), \tag{5.15b}$$
$$\theta = \arccos(1-2p) = 2\arcsin(\sqrt{p}). \tag{5.15c}$$

The transition probability reads

$$P = [1 - \sin^4(\epsilon/2)]\sin^2(\theta/2). \tag{5.16}$$

It is obviously accurate up to order $O(\epsilon^4)$.

The sequence (5.14) is derived as follows. First, we calculate the overall propagator of Eq. (5.3) for $N = 3$ pulses. Numerical evidence suggests that the pulse areas could be taken as in Eq. (5.14), i.e. a π pulse in the middle sandwiched by two half-π pulses. We take the first phase to be 0, and we are left with two phases to be determined. The overall three-pulse transition probability for zero error ($\epsilon = 0$) is readily calculated to be

$$P = |U_{21}|^2 = \sin^2(\phi_2 - \phi_3/2). \tag{5.17}$$

If we set $P = \sin^2(\theta/2)$ (as for a resonant θ pulse), we find $\phi_3 = 2\phi_2 - \theta$. Next we calculate the first few derivatives of U_{21} with respect to the error ϵ and find

$$U'_{21}(\epsilon = 0) = 0, \tag{5.18}$$
$$U''_{21}(\epsilon = 0) = [1 + 2\cos(\theta) + 2\cos(\phi_2) + 2\cos(\theta - \phi_2) + \cos(\theta - 2\phi_2)]/8, \tag{5.19}$$
$$U'''_{21}(\epsilon = 0) = 0. \tag{5.20}$$

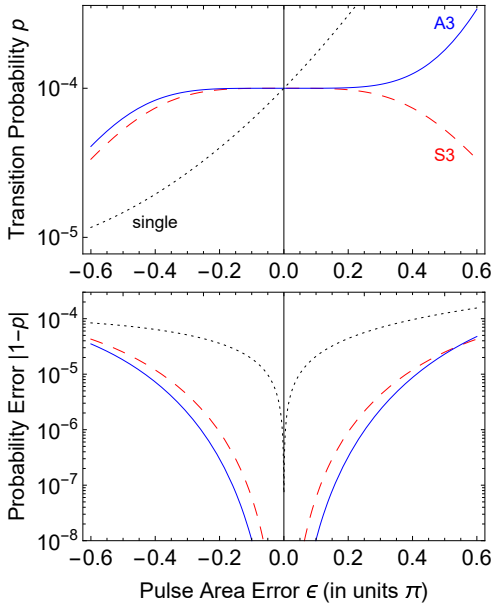

Figure 5.2: Performance of the three-pulse composite sequences (5.14) (red dashed) and (5.22) (blue solid) for the transition probability $p = 10^{-4}$. The dotted curves show the single pulse excitation probability for comparison.

p	A_1	A_2	A_3	ϕ_2	ϕ_3
10^{-2}	0.5682	1.2436	0.6292	1.1533	0.2546
10^{-3}	0.5904	1.2276	0.6232	1.0785	0.1405
10^{-4}	0.6001	1.2229	0.6184	1.0419	0.0785
10^{-5}	0.6049	1.2214	0.6151	1.0229	0.0441
10^{-6}	0.6074	1.2209	0.6131	1.0126	0.0248
10^{-7}	0.6087	1.2208	0.6119	1.0070	0.0139
10^{-8}	0.6094	1.2207	0.6113	1.0039	0.0078

Table 5.2: Pulse areas and phases (in units of π) for the composite sequences of 3 pulses (5.22) for a few values of the transition probability p. All composite sequences have the error order $O(\epsilon^5)$.

The vanishing of the odd-order derivatives follows from the choice of symmetric pulse areas in Eq. (5.14). By setting $\phi_2 = \theta/2 + \beta$ the equation for $U''_{21}(\epsilon = 0)$ reduces to

$$2\cos\beta\cos(\theta/2) + \cos^2\beta + \cos\theta = 0. \tag{5.21}$$

has 4 solutions, two complex and two real, of which one positive and one negative. The real positive solution is given by the expression listed in Eq. (5.14). The first nonzero derivative is $U^{(4)}_{21}(\epsilon = 0)$. The availability of analytic formulae for the phases allows us to find their values for any value of the transition probability.

5.3.2.2 *Asymmetric sequence of pulses*

The most general three-pulse composite sequence has the form

$$A3: \quad (A_1)_0(A_2)_{\phi_2}(A_3)_{\phi_3}. \tag{5.22}$$

Although the composite sequence (5.22) costs more total pulse area ($\approx 2.44\pi$) than the preceding two, it is accurate to order $O(\epsilon^5)$. The pulse areas and the phases computed numerically are given in Table 5.2.

The performance of the three-pulse sequences is illustrated in Fig. 5.2. Both sequences (5.14) and (5.22) outperform both the conventional single-pulse excitation probability and the two-pulse composite sequences (5.7) and (5.11) of Fig. 5.1. Moreover, the asymmetric sequence A3 of Eq. (5.11), which is of error order $O(\epsilon^5)$, clearly outperforms the symmetric sequence S3 of Eq. (5.14), which is of error order $O(\epsilon^4)$.

Because the three-pulse sequences seem to be the "sweet spot" in terms of performance (error order and high-fidelity window width) versus cost (total pulse area and control complexity), they deserve some discussion. There are clear advantages and disadvantages of each of these two sequences. The S3 sequence has a nice analytic form and a total pulse area of 2π. However, it has lower error order than A3. The real advantage of the sequence S3 is its analytic form, which makes it very easy to calculate the composite phases for any target transition probability p. The A3 sequence looks less attractive as neither the pulse area nor the phases are rational numbers and they are all numerical, but this sequence has the higher order of error compensation, although at the expense of the larger pulse area of about 2.44π. Its real inconvenience is in the fact that for target transition probabilities not listed in Table 5.2 one has to calculate them numerically, although this is not a very difficult task.

5.3.3 *Four-pulse composite sequences*

The most general four-pulse composite sequence has the form

$$(A_1)_0(A_2)_{\phi_2}(A_3)_{\phi_3}(A_4)_{\phi_4}. \tag{5.23}$$

We present three sets of four-pulse composite sequences, two symmetric and one asymmetric.

5.3.3.1 *Symmetric sequences of pulses*

The first symmetric sequence consists of identical nominal $\pi/2$ pulses (but with different phases) [152],

$$S4a: \quad (\tfrac{1}{2}\pi)_0(\tfrac{1}{2}\pi)_{\frac{1}{2}\pi}(\tfrac{1}{2}\pi)_{\frac{3}{2}\pi-\theta}(\tfrac{1}{2}\pi)_{\pi-\theta}, \tag{5.24}$$

where $\theta = 2\arcsin\sqrt{p}$. Its total pulse area is just 2π. The overall transition probability reads

$$P = p[1-\sin^4(\pi\epsilon/2)]. \tag{5.25}$$

Obviously, it is accurate up to order $O(\epsilon^4)$.

The other symmetric sequence of pulses reads [152]

$$S4b: \quad (\tfrac{1}{2}\pi)_0\pi_{\frac{2}{3}\pi}\pi_{\frac{5}{3}\pi-\theta}(\tfrac{1}{2}\pi)_{\pi-\theta}. \tag{5.26}$$

The overall transition probability reads

$$P = p[1-\sin^6(\pi\epsilon/2)]. \tag{5.27}$$

Obviously, in return to the larger total pulse area ot 3π compared to the previous sequence (5.24) it is accurate up to the higher order $O(\epsilon^6)$.

These sequences are very convenient as the availability of exact analytic formulae for the phases allows us to find their values for any value of the transition probability.

5.3.3.2 *Asymmetric sequences*

The most general three-pulse composite sequence has the form

$$A4: \quad (A_1)_0(A_2)_{\phi_2}(A_3)_{\phi_3}(A_4)_{\phi_4}. \tag{5.28}$$

All pulse areas and phases are free control parameters, which allow it to compensate a higher error order. The pulse areas and the phases are computed numerically and are listed in Table 5.3. Although the asymmetric composite sequence (5.28) costs more total pulse area ($\approx 3.44\pi$) than the preceding two sequences S4a and S4b, it is accurate to the higher order $O(\epsilon^7)$.

The performance of the four-pulse sequences is illustrated in Fig. 5.3. All of them significantly outperform the single pulse profile and provide considerable stabilisation at the target transition probability value. The best performance is delivered by the asymmetric sequence A4, which has the error order $O(\epsilon^7)$, followed by S4b, with the error order $O(\epsilon^6)$, and then S4a, with the error order $O(\epsilon^4)$. However, this ranking follows the total pulse area — the cost factor — which is $\approx 3.41\pi$ for A4, 3π for S4b,

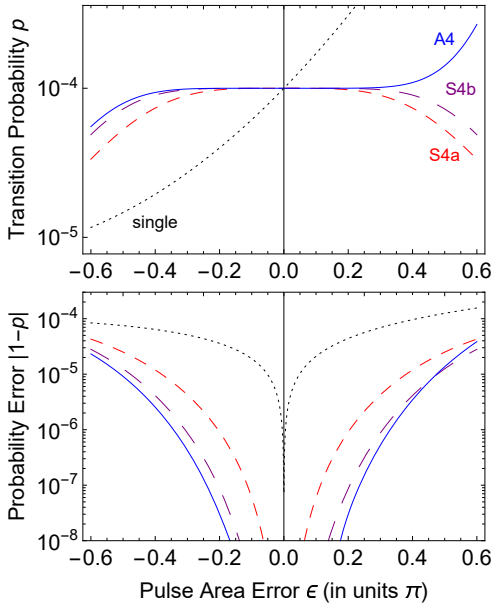

Figure 5.3: Performance of the four-pulse symmetrci composite sequences (5.24) (red dashed), (5.26) (purple long-dashed) and the asymmetric sequence (5.28) (blue solid) for the transition probability $p = 10^{-4}$. The dotted curves show the single pulse excitation probability for comparison.

p	A_1	A_2	A_3	A_4	ϕ_2	ϕ_3	ϕ_4
10^{-2}	0.5367	1.1586	1.1360	0.5833	0.8499	1.5547	0.4360
10^{-3}	0.8685	1.0434	0.3702	0.5174	1.0634	0.8847	0.0128
10^{-4}	0.8165	0.9044	0.5579	0.6423	1.0362	0.9682	0.0146
10^{-5}	0.7854	0.8335	0.6433	0.6905	1.0207	0.9856	0.0090
10^{-6}	0.7669	0.7937	0.6875	0.7141	1.0118	0.9926	0.0052
10^{-7}	0.7551	0.7698	0.7108	0.7255	0.9933	1.0042	1.9972
10^{-8}	0.7494	0.7578	0.7244	0.7328	0.9962	1.0022	1.9984

Table 5.3: Pulse areas and phases (in units of π) for the composite sequences of 4 pulses (5.28). All composite sequences have the error order $O(\epsilon^7)$.

and 2π for S4a. Note that the error order $O(\epsilon^4)$ for S4a is the same as the one for the three-pulse sequence $S3$ and one can verify that they generate similar excitation profiles.

5.3.4 *Higher number of pulses*

Higher number of pulses present the opportunity for an error compensation of a higher order. There exist analytic symmetric composite sequences for arbitrary rotations, which can be used for small p too [152]. They are constructed as follows. We can use a composite $\pi/2$ pulse to derive a composite θ-pulse by applying a composite $\pi/2$

pulse sequence C, followed by the composite sequence C_θ^R, which is the time-reversed sequence C, with all its phases shifted by the same phase shift θ,

$$C_0 C_\theta^R, \tag{5.29}$$

an idea introduced by Levitt and Ernst [72]. Moreover, if the sequence C has the error order $O(\epsilon^n)$ then the composite θ sequence (5.29) has the error order $O(\epsilon^{2n})$ [152]. A few examples follow.

The composite sequence S2 of Eq. (5.7) becomes a composite $\pi/2$ pulse for $\theta = \pi/2$, which can be used in the twinning construction (5.29),

$$(\tfrac{1}{2}\pi)_0(\tfrac{1}{2}\pi)_{\frac{1}{2}\pi}(\tfrac{1}{2}\pi)_{\frac{3}{2}\pi-\theta}(\tfrac{1}{2}\pi)_{\pi-\theta}, \tag{5.30}$$

which is the same as the sequence S4a of Eq. (5.24). Because the sequence S2 has the error order $O(\epsilon^2)$ then the composite sequence S4a has the error order $O(\epsilon^4)$, as found in the previous section.

The composite sequence S3 of Eq. (5.14) for $\theta = \pi/4$ reads

$$(\tfrac{1}{2}\pi)_0\pi_{\frac{3}{4}\pi}(\tfrac{1}{2}\pi)_\pi, \tag{5.31}$$

and it has the error order $O(\epsilon^4)$. By using the twinning construction (5.29) we find a θ composite sequence of order $O(\epsilon^8)$,

$$(\tfrac{1}{2}\pi)_0\pi_{\frac{3}{4}\pi}(\tfrac{1}{2}\pi)_\pi(\tfrac{1}{2}\pi)_{2\pi-\theta}\pi_{\frac{7}{4}\pi-\theta}(\tfrac{1}{2}\pi)_{\pi-\theta}. \tag{5.32}$$

One can build θ composite sequences of arbitrary length and arbitrary error order compensation by twinning the $\pi/2$ composite sequences [152]

$$(\pi/2)_0\pi_{\phi_2}\pi_{\phi_3}\cdots\pi_{\phi_{N-1}}(\pi/2)_{\phi_N}, \tag{5.33}$$

composed of a sequence of $N-2$ nominal π pulses, sandwiched by two pulses of areas $\pi/2$, with phases given by the analytic formula

$$\phi_k = \frac{(k-1)^2}{2(N-1)}\pi \quad (k = 1, 2, \ldots, N). \tag{5.34}$$

It is easy to verify that the sequences (5.30) and (5.32) (after trivial population-preserving transformation of the phases) belong to such a family of sequences. Because the sequence (5.33) has the error order $O(\epsilon^{2(N-1)})$ the corresponding twinned sequence (5.29) will have the error order $O(\epsilon^{4(N-1)})$.

Another, asymmetric family of $\pi/2$ composite sequences can be used too [152],

$$(\pi/2)_0\pi_{\phi_2}\pi_{\phi_3}\cdots\pi_{\phi_{N-1}}(\pi)_{\phi_N}, \tag{5.35}$$

composed of a sequence of $N-1$ nominal π pulses, preceded by a nominal $\pi/2$ pulse, with phases given by the analytic formula

$$\phi_k = \frac{2(k-1)^2}{2N-1}\pi \quad (k = 1, 2, \ldots, N). \tag{5.36}$$

It has the error order $O(\epsilon^{2N-1})$. Hence the twinning method (5.29) generates θ sequences of the error order $O(\epsilon^{2(2N-1)})$. For instance, for $N = 3$ we find by twinning the θ sequence

$$(\tfrac{1}{2}\pi)_0\pi_{\frac{2}{5}\pi}(\pi)_{\frac{8}{5}\pi}(\pi)_{\frac{3}{5}\pi-\theta}\pi_{\frac{7}{5}\pi-\theta}(\tfrac{1}{2}\pi)_{\pi-\theta}, \tag{5.37}$$

which has the error order $O(\epsilon^{10})$.

Regarding the asymmetric composite sequences of 2, 3 and 4 pulses, presented above and derived numerically, it is computationally much harder to derive similar sequences for more than 4 pulses. Moreover, the advantage they deliver in terms of error order compensation for a given number of pulses compared to the symmetric sequences seems to decrease with the number of pulses N and approach the point when the results do not repay the labour.

5.4 QUANTUM GATES FOR ULTRASMALL ROTATIONS

Ultrasmall rotation gates are more demanding to construct due to the necessity to have both the probabilities and the phases error-compensated. Mathematically, this is equivalent to expanding the propagator of the gate in a Taylor-Maclaurin series versus the error ϵ and set to zero the first few terms to the same error order $O(\epsilon^m)$ in all propagator matrix elements. Below we present several sequences, which produce high-fidelity rotation gates, two of which are known in the literature and one is derived here.

5.4.1 *First-order error compensation*

The three-pulse rotation gate has been derived by Wimperis [73],

$$W3: \quad \theta_0\pi_\phi\pi_{3\phi}, \tag{5.38}$$

Rotation gate G3: $(\frac{1}{2}\pi + x)_{\phi_1}\pi_{\pi+y}(\frac{1}{2}\pi + x)_{\phi_1}$			
p	x	ϕ_1	y
10^{-2}	2.5×10^{-3}	2.492×10^{-2}	5.672×10^{-2}
10^{-3}	2.5×10^{-4}	7.904×10^{-3}	1.797×10^{-2}
10^{-4}	2.5×10^{-5}	2.500×10^{-3}	5.683×10^{-3}
10^{-5}	2.5×10^{-6}	7.906×10^{-4}	1.797×10^{-3}
10^{-6}	2.5×10^{-7}	2.500×10^{-4}	5.684×10^{-4}

Table 5.4: Parameters of the composite sequence G3 of Eq. (5.39) for different transition probabilities p.

with $\theta = \arccos(1-2p) = 2\arcsin\sqrt{p}$ and $\phi = \arccos(-\theta/(2\pi)) \approx \frac{1}{2}\pi + \sqrt{p}$. It is accurate up to order $O(\epsilon^2)$. It is a phase-distortionless sequence and hence suitable for a rotation gate.

Another three-pulse rotation gate has the form [43]

$$G3: \quad \alpha_{\phi_1}\pi_{\phi_2}\alpha_{\phi_1}, \tag{5.39}$$

where α is determined from the equation

$$\frac{\pi\sin(\alpha)}{\alpha} = 2\cos(\theta/2). \tag{5.40}$$

Given α, we can find ϕ_1 and ϕ_2 from

$$2\alpha\cos(\phi_1 - \phi_2) + \pi = 0, \tag{5.41a}$$

$$\sin(\phi_1 - \phi_2) = \sin(\theta/2)\cos(\phi_1). \tag{5.41b}$$

This composite sequence is related to the SCROFULOUS composite pulse [153] and it is accurate to the error order $O(\epsilon^2)$.

The values of the pulse area and the composite phases are given in Table 5.4.

5.4.2 *Second-order error compensation*

A well-known composite seqeunce, which compensates the second-order error is the BB1 sequence of Wimperis [37],

$$\text{BB1} = (\pi/2)_0\pi_\chi(2\pi)_{3\chi}\pi_\chi, \tag{5.42}$$

with $\chi = \arccos(-\theta/4\pi)$. It produces arbitrary phase-distortionless rotations at the angle θ with the error order $O(\epsilon^3)$

5.5 CONCLUSIONS

We presented a solution to the problem of generating well-defined very small excitation of a two-state quantum transition. The method uses composite pulse sequences of two, three, four and more pulses. Both symmetric and asymmetric, analytic and numeric classes of sequences have been presented and analyzed in detail.

The results in this paper can be useful in application such as single-photon generation by a cold atomic ensemble of N atoms. A composite sequence producing a transition probability of $1/N$ will make sure that only one excitation is shared within the ensemble, to be subsequently released by a scheme like DLCZ. Another possible application is fine tuning of quantum gates, in which accurate small adjustments of the rotation angle are needed in order to reach high fidelity. Yet another application is the generation of huge Dicke states in cold atomic ensembles or trapped ions by global collective addressing.

6

COMPOSITE PULSES FOR ULTRAROBUST OR ULTRASENSITIVE CONTROL

6.1 INTRODUCTION AND MOTIVATION

Based on this concept of CPs for rotations on the Bloch space, Ardavan proposed to use the so-called BB1 or BB2 sequences for polarization retarders (i.e., rotations on the Poincaré sphere) [154]. Existence of BB2 and NB2 sequences leads to the idea of altering CPs, which improve the feature (BB or NB) of the pulse at the expense of precision due to alternations (inflection points) on the top (BB) or on the bottom (NB) of the errant transition probability. We call these new subclasses of CPs as ultrabroadband and ultranarrowband respectively.

With novel method (see Sec. 6.3) we have derived ultrabroadband and ultranarrowband CPs [47], when $\theta = \pi$. These CPs are useful in the applications, where high-accuracy (about 90%) is enough (although higher precision can be achieved increasing number of pulses, due to the novel method).

6.2 JONES MATRICES AND ON THE QUANTUM-CLASSICAL ANALOGY

Jones polarization matrix for a retarder with a phase shift φ (the phase shift applied between the ordinary and the extraordinary ray passing through the retarder) and rotated at an angle η is given as (in the left-right circular polarization basis)

$$\mathbf{J}_\eta(\varphi) = \begin{bmatrix} \cos\left(\frac{\varphi}{2}\right) & i\sin\left(\frac{\varphi}{2}\right)e^{2i\eta} \\ i\sin\left(\frac{\varphi}{2}\right)e^{-2i\eta} & \cos\left(\frac{\varphi}{2}\right) \end{bmatrix}. \tag{6.1}$$

For example, half- and quarter-wave plates rotated at an angle η, i.e. $(\lambda/2)_\eta$, $(\lambda/4)_\eta$, are described by $\mathbf{J}_\eta(\pi)$ and $\mathbf{J}_\eta(\pi/2)$ respectively.

Polarization retarder is equivalent to x-rotation or quantum rotation gate, and polarization rotator is equivalent to z-rotation or quantum phase gate. Henceforward, we

will use NMR QC terminology and notation, and the results for PO can be obtained by abovementioned way.

6.3 DERIVATION METHOD

So, errant overall propagator is SU(2) matrix. Let's consider the general form for general composite rotation

$$\mathbf{U}_n(\epsilon) = \begin{bmatrix} \exp(-i\zeta_\epsilon/2)\cos(\theta_\epsilon/2) & -i\sin(\theta_\epsilon/2)\exp(i\phi_\epsilon) \\ -i\sin(\theta_\epsilon/2)\exp(-i\phi_\epsilon) & \exp(i\zeta_\epsilon/2)\cos(\theta_\epsilon/2) \end{bmatrix}. \tag{6.2}$$

For rotational θ pulses parameters follows $\theta_{\epsilon=0} = \theta$, $\zeta_{\epsilon=0} = 0$ and $\phi_{\epsilon=0} = \phi$ ($\phi = 0$ is the case for ideal θ pulse), and for phasal ζ pulses parameters are equal $\zeta_{\epsilon=0} = \zeta$, $\theta_{\epsilon=0} = 0$ and $\phi_{\epsilon=0} = const$.

Note that derivation method presented in Subsec. 6.3.1 does not care about rotation angle, geometric and relative phase stabilities. Here, we have deal with alternating CPs, which make the feature (robustness/sensitivity or both) of the pulse more powerful, sometimes called *ultra*, at the expense of precision due to alternations (at the center/ on the wings or both).

6.3.1 *Ultra-BB, ultra-NB and ultra-PB*

6.3.1.1 *Case of rotational θ pulses*

Let's maximize the population transfer area (6.3) at the whole-range of the error bandwidth, i.e. from $\epsilon = -1$ to $\epsilon = 1$ (ultrabroadband θ pulses)

$$\sum\nolimits_{b,n} \stackrel{\Delta}{=} \int_{-1}^{1} p(\epsilon)\, d\epsilon, \tag{6.3}$$

or minimize it (ultranarrowband θ pulses).

In (6.3) $p(\epsilon = 0) = p(\theta = \pi) = \sin^2\theta/2|_{\theta=\pi} = 1$, at the center of bandwidth, is transition probability in QC: when pulse area error is zero, the qubit-state completely transfers from $|0\rangle$ to $|1\rangle$ due to π-rotation on the Bloch sphere. In PO this is mathematically equivalent (see Subsec. 6.2) to the conversion of the polarization state from $|L\rangle$ to $|R\rangle$ (or $|H\rangle$ to $|V\rangle$) due to π-rotation on the Poincaré sphere

$$\int_0^{2\pi} I(\varphi')\, d\varphi' = \int_0^{2\pi} |\mathcal{U}_{12}(\varphi')|^2\, d\epsilon, \tag{6.4}$$

and $I(\varphi')$ describes the conversion efficiency of the half-wave plate $I(\varphi' = \pi) = 1$.

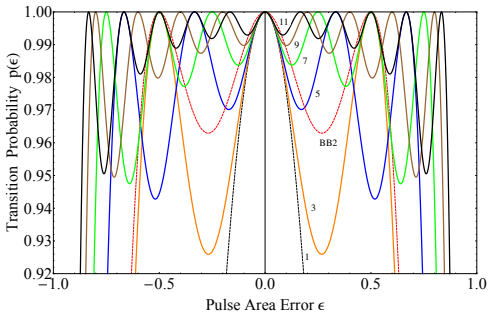

Figure 6.1: Transition probability $p(\epsilon)$ of ultrabroadband rotational π pulses. The numbers N on the curves refer to CP sequences UBN listed in the Table 6.1 in the main thesis. As noted above, the curves have $k = N - 1$ alternations on the top of the plot, unlike the BB2 sequence, which has 2 alternations, so it's worse than our five-π UB5.

6.3.1.2 *Case of phasal ζ pulses*

Let's maximize the phase shifting area (6.5) at the whole-range of the error bandwidth, i.e. from $\epsilon = -1$ to $\epsilon = 1$ (ultrabroadband ζ pulses)

$$\sum \stackrel{\Delta}{=} \int_{-1}^{1} z(\epsilon)\, d\epsilon. \tag{6.5}$$

Here the phase shifting $z(\epsilon)$ is equal to the trace fidelity in our case $\zeta = \pi$

$$\mathcal{F}_{\mathrm{T}} = \tfrac{1}{2}\mathrm{Tr}\left[\mathbf{U}_n(\epsilon)\mathbf{U}_n{}^{\dagger}\right] = \cos\left(\frac{\zeta - \zeta_\epsilon}{2}\right)_{\zeta=\pi} \cos\left(\frac{\theta_\epsilon}{2}\right) = \sin\left(\frac{\zeta_\epsilon}{2}\right)\cos\left(\frac{\theta_\epsilon}{2}\right), \tag{6.6}$$

and the target matrix is

$$\mathbf{U}_n = \begin{bmatrix} \exp(-i\zeta/2) & 0 \\ 0 & \exp(i\zeta/2) \end{bmatrix}_{\zeta=\pi} = \begin{bmatrix} -i & 0 \\ 0 & i \end{bmatrix}. \tag{6.7}$$

6.4 ULTRABROADBAND ROTATIONAL $\theta = \pi$ PULSES

The most convenient way to construct ultrabroadband rotational π pulses is the symmetric design consisting of nominal π pulses

$$\pi_{\phi_1}\pi_{\phi_2}\ldots,\pi_{\phi_{k/2}}\pi_{\phi_{k/2+1}}\pi_{\phi_{k/2}}\ldots\pi_{\phi_2}\pi_{\phi_1}, \tag{6.8}$$

where $k = N - 1$ is the number of inflection points in the errant transition probability vs the pulse area error plot (the number of alternations of the plot).

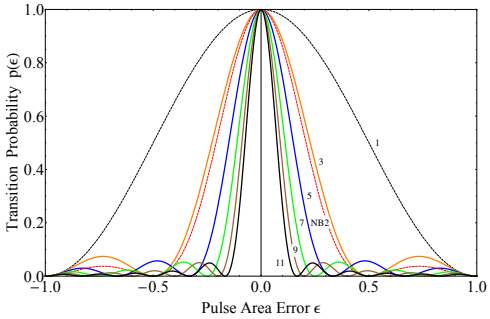

Figure 6.2: Transition probability $p(\epsilon)$ of ultranarrowband rotational π pulses. The numbers N on the curves refer to CP sequences UNN listed in the Table 6.2 in the main thesis. As noted above, the curves have $k = N - 1$ alternations on the bottom of the plot, unlike the NB2 sequence, which has 2 alternations, so it's worse than our five-π UN5.

We have derived up to eleven sequences, which increase the broadness range of the original rotational sequence (a single pulse) more than four times (from 20.5% to 87.7%), and the transition probability area is increased by 83.(3)% by the eleven-π UB11 sequence. Composite phases for the ultrabroadband rotational pulses are shown in the Table 6.1 in the main thesis, and the transition probability is plotted in Figure 6.1.

6.5 ULTRANARROWBAND ROTATIONAL $\theta = \pi$ PULSES

Since NB pulses are asymmetric in composite phases, to construct ultranarrowband rotational π pulses we choose the antisymmetric design consisting of nominal π pulses

$$\pi_{\phi_1}\pi_{\phi_2}\ldots,\pi_{\phi_{k/2}}\pi_{\phi_{k/2+1}}\pi_{-\phi_{k/2}}\ldots\pi_{-\phi_2}\pi_{-\phi_1}, \tag{6.9}$$

where $k = N - 1$ is the number of inflection points in the errant transition probability vs the pulse are error plot (the number of alternations of the plot). For convenience, the middle phases can be taken as $\phi_{k/2+1} = \pi$.

We have derived up to eleven sequences, which decrease the narrowness range at 50% of probability, viz. full width at half maximum (FWHM), of the original rotational sequence (a single pulse) about 6.75 times (from 50% to 7.4%), and the transition probability area is decreased by 83.(3)% by the eleven-π UN11 sequence. Composite phases for the ultranarrowband rotational pulses are shown in the Table 6.2 in the main thesis, and the transition probability is plotted in Figure 6.2.

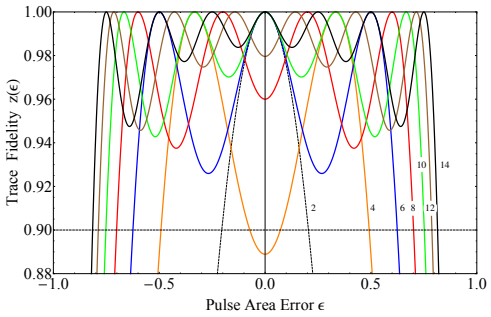

Figure 6.3: Trace fidelity $z(\epsilon)$ of ultrabroadband phasal π pulses. The numbers N on the curves refer to CP sequences UBPhN listed in the Table 6.3 in the main thesis. As noted above, the curves have $k = N - 2$ alternations on the top of the plot.

6.6 ULTRABROADBAND PHASAL $\zeta = \pi$ PULSES

As usual (cf. (3.3)), we construct ultrabroadband phasal π pulses with asymmetric design consisting of nominal π pulses

$$\pi_{\phi_1}\pi_{\phi_2}\ldots\pi_{\phi_{k/2+1}}\cdot\pi_{\phi_1+\frac{1}{2}\pi}\pi_{\phi_2+\frac{1}{2}\pi}\ldots\pi_{\phi_{k/2+1}+\frac{1}{2}\pi}, \tag{6.10}$$

where $k = N - 2$ is the number of inflection points in the trace fidelity vs the pulse are error plot (the number of alternations of the plot).

We have derived up to fourteen sequences, which increase the broadness range of the original phasal sequence (two pulses) about four times (from 20.5% to 81.5%), and the trace fidelity area is increased by the 75% by the fourteen-π UBPh14 sequence. Composite phases for the ultrabroadband phasal pulses are shown in the Table 6.3 in the main thesis, and the trace fidelity is plotted in Figure 6.3.

6.7 COMMENTS AND CONCLUSIONS

We presented a number of CP sequences consisting of π pulses for transition of the quantum state from $|0\rangle$ to $|1\rangle$ in ultrarobust and ultrasensitive manners, according to the pulse area deviation ϵ. Using quantum-classical analogy, we presented a number of sequences of half-wave plates for conversion of the polarization state from $|H\rangle$ to $|V\rangle$ or from $|L\rangle$ to $|R\rangle$ in ultrabroadband and ultranarrowband ways, according to the phase-shift (retardation) deviation $\varphi\prime - \varphi = \varphi\prime - \pi$. Our longest UB11 pulse covers approximately 88% of the whole width for the same benchmark. Our longest UNB11 pulse covers approximately 21% of the whole width for the same benchmark. We theoretically design ultrarobust Z quantum gate via a number of CP sequences consisting of π pulses, and equivalently ultrabroadband polarization π rotator. Our longest UBPh14 pulse maintains 90% of trace fidelity over a broadness range of roughly 1.63π.

7

BROADBAND COMPOSITE NONRECIPROCAL POLARIZATION WAVE PLATES AND OPTICAL ISOLATORS

7.1 INTRODUCTION

The analogy between the polarization Jones vector and the quantum state vector has recently been used to suggest arbitrarily precise broadband polarization retarders [7, 8, 154]. As recently shown by Al-Mahmoud et. al [155], wave plates retarders can be non-reciprocal whose phase-shift retardation depends on the light propagation direction.

In this chapter, we theoretically propose novel broadband polarization quarter-wave plates, which are also nonreciprocal, with the potential to be used in broadband optical isolators or/and circulators for telecommunications, industrial, and laboratory research.

7.2 BACKGROUND

Another way to realize a retarder is to use a polarization rotator at an angle θ sandwiched in between two quarter-wave plates rotated by angles $-\pi/4$ and $\pi/4$ with respect to the lab reference frame correspondingly [156]. The Jones matrix J for such a sequence can be given by the product of the Jones matrices of the quarter-wave plates and the rotator:

$$J = J_{-\pi/4}(\pi/2)\, R(\theta)\, J_{\pi/4}(\pi/2) = \begin{bmatrix} e^{i\theta} & 0 \\ 0 & e^{-i\theta} \end{bmatrix} = J_0(2\theta)\,. \tag{7.1}$$

The last part of Eq. (7.1) demonstrates that the whole sequence can be considered an effective wave plate with an effective retardation $\varphi = 2\theta$. If one uses Faraday rotator (nonreciprocal device) then the effective waveplate is also nonreciprocal [155].

7.3 COMPOSITE WAVE PLATE

Now we will show three different sequences of non-reciprocal elements to construct nonreciprocal broadband quarter-wave plates:

$$\mathcal{J}(\varepsilon) = J_{\alpha_1}(\pi/2+\varepsilon/2)\, J_{\alpha_2}(\pi+\varepsilon)\, J_{\alpha_3}(\pi/2+\varepsilon/2), \tag{7.2}$$

$$\mathcal{J}(\varepsilon) = J_{\alpha_1}(\pi+\varepsilon)\, J_{\alpha_2}(\pi+\varepsilon)\, J_{\alpha_3}(\pi/2+\varepsilon/2), \tag{7.3}$$

$$\begin{aligned}\mathcal{J}(\varepsilon) = {} & J_{\alpha_1}(\pi+\varepsilon)\, J_{\alpha_2}(\pi+\varepsilon)\, J_{\alpha_3}(\pi+\varepsilon) \\ & \times J_{\alpha_4}(\pi+\varepsilon)\, J_{\alpha_5}(\pi/2+\varepsilon/2).\end{aligned} \tag{7.4}$$

For the above odd number of sequences (7.2)-(7.4) one can easily check that they are nonreciprocal.

In order to produce broadband nonreciprocal quarter-wave plate we determine the rotation angles of each wave plate in Eqs. (7.2), (7.3) or (7.4) by using the Monte Carlo method. We select solutions, which deliver the biggest overall fidelity $\mathfrak{F}(\varepsilon)$ in the interval of $\varepsilon \in [-\pi, \pi]$ and also, ensure a flat top. The angles are presented in the Table 7.1.

Table 7.1: Calculated angles of rotation (in radians) for the three sequences of Eqs. (7.2), (7.3), and (7.4).

sequences	angles $(\alpha_1; \alpha_2; \ldots; \alpha_N)$
(7.2)	(3.3; 1.21; 3.1)
(7.3)	(3.6; 1.65; 3.9)
(7.4)	(1.61;6.48;6.47;1.62;0.78)

7.4 BROADBAND OPTICAL ISOLATOR

Another interesting case is when the sequence serves as a broadband null retarder in one direction and a broadband half-wave plate in the other direction, which can be archived if we combine our nonreciprocal broadband quarter-wave plate with a commercially available broadband but reciprocal quarter-wave plate. In this case, one can build a broadband optical isolator as shown and explained in Figure 7.1.

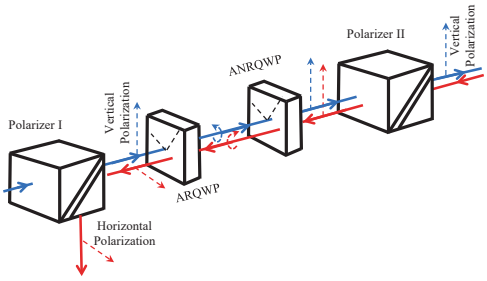

Figure 7.1: Scheme of the broadband optical isolator. ARQWP stands for the achromatic reciprocal quarter-wave plate, while ANRQWP stands for the achromatic nonreciprocal quarter-wave plate.

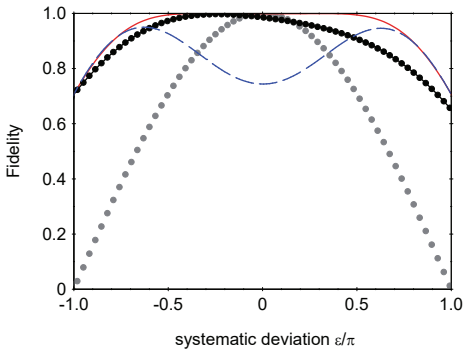

Figure 7.2: Fidelity versus systematic deviation for the composite waveplates designed by using three configurations: Eq. (7.2) is depicted by the blue dashed line, Eq. (7.3) by the black dotted line, and Eq. (7.4) by the red solid line. The gray dotted line is for a quarter-wave plate with a single Faraday rotator for easy reference.

7.5 NUMERICAL CALCULATIONS

In Figure 7.2 we show the calculation for the fidelity $\mathfrak{F}$ profiles using the three configurations (7.2), (7.3) and (7.4) with rotation angles taken from the Table 7.1.

For broadband optical isolator simulations in this chapter, we use terbium gallium garnet crystal (TGG) as it is one of the most common crystals for Faraday rotators. We fix the applied magnetic field to 1 T, the length of the crystal is considered to be 1 cm for the half-wave plates and 0.5 cm for the quarter-wave plates. Up until now, there has been a lot of research done on the dispersion of the TGG Verdet constant ν [157–159].

The performance of the optical isolators is quantified by its transmission T_f (a portion of the input light's intensity that passes through the isolator), back-transmission T_b (a portion of the back-transmission light's intensity that passes through the isolator in the opposite direction), and isolation D.

The transmission and isolation profiles for the three configurations (7.2), (7.3) and (7.4) are shown in Figures 7.3 and 7.4. One can notice that for all these composite isolators both the transmission and isolation are far more efficient than that of isolators

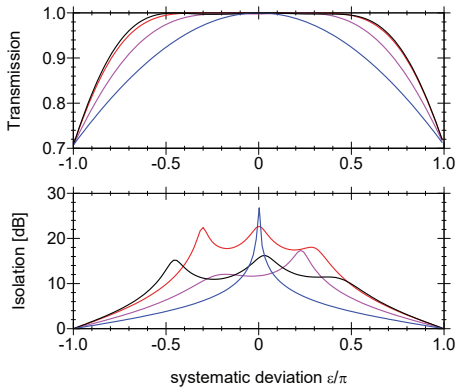

Figure 7.3: Transmission and isolation properties of the optical isolators with different numbers of wave plates in the series, compared to the isolator based on a single rotator (blue line), vs the systematic deviation ε. The other three curves refer to the sequences of Eqs. (7.2) depicted by a purple line, (7.3) by a red line, and (7.4) by a black line.

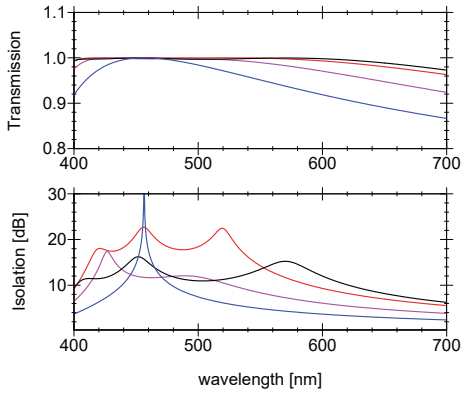

Figure 7.4: The same as Figure 7.3 but instead of systematic deviation ε we use the wavelength parameter.

using a single rotator (blue curve). The isolation above 10 dB over a region of 200 nm can be seen from Figure 7.4, and it is a much broader spectral range compared to the case of using just a single Faraday rotator (about 20 nm on the level of 10 dB).

7.6 CONCLUSIONS

We have presented a novel way to construct broadband nonreciprocal polarization quarter-wave plates. The proposed broadband nonreciprocal polarization quarter-wave plate can be used in combination with a broadband reciprocal polarization quarter-wave plate to build a broadband optical isolator.

8

GENERAL CONCLUSIONS AND PERSPECTIVES

Composite pulses, the powerful quantum control technique from nuclear magnetic resonance, and its wide applications have been explored in this thesis, which are novel or have not been reported in the literature hitherto. The dissertation exhibits the delicate susceptibility of the method to mathematically different kinds of target problems. The prime purpose of the thesis is to encourage a wide range of researchers in both classical and quantum physics to leverage this magical and versatile technique to their research tasks. Thesis addresses several specialized applications, namely in quantum computing and quantum information, quantum information processing (quantum cryptography and quantum networks), quantum sensing, and polarization optics.

We presented a number of this kind of broadband phase-distorionless composite pulse sequences for three basic quantum gates — the X gate, the Hadamard gate and arbitrary rotation gates in Chapter 2. In the same fashion, we presented a number of broadband phase-distortionless composite pulse sequences for four basic quantum gates — the Z gate, the S gate, the T gate and arbitrary phase gates in Chapter 3. We derived narrowband and passband composite rotational quantum gates — the X gate, the Hadamard gate and arbitrary rotation gates in Chapter 4. Robust ultrasmall transition probability composite pulses, which are the subject of Chapter 5, allow to construct deterministic and highly efficient single-photon source. Derivation methodology and capabilities of ultrabroadband-type (ultrarobust) and ultranarrowband-type (ultrasensitive) types of composite pulses is presented in Chapter 6. In Chapter 7 we presented a novel way to construct broadband nonreciprocal polarization quarter-wave plates via composite pulse parameters.

A

PUBLICATIONS AND PRESENTATIONS

A.1 PUBLICATIONS

1. Hayk L. Gevorgyan and Nikolay V. Vitanov, "**Ultrahigh-fidelity composite rotational quantum gates**" published in *Physical Review A*, **104** (1), 012609 (2021), DOI: 10.1103/physreva.104.012609.

2. Hayk L. Gevorgyan and Nikolay V. Vitanov, "**Ultrahigh-fidelity composite quantum phase gates**", arXiv:2306.10340 [quant-ph], DOI: 10.48550/arXiv.2306.10340.

3. Hayk L. Gevorgyan and Nikolay V. Vitanov, "**Deterministic generation of arbitrary ultrasmall excitation of quantum systems by composite pulse sequences**", arXiv:2306.13209 [quant-ph], DOI: 10.48550/arXiv.2306.13209

4. Hayk L. Gevorgyan and Nikolay V. Vitanov, "**Narrowband and passband composite rotational quantum gates**", to be submitted for publication.

5. Hayk L. Gevorgyan, "**Ultrabroadband and Ultranarrowband Composite Polarization Half-Waveplates**" published in *Optica High-brightness Sources and Light-driven Interactions Congress 2022*, Technical Digest Series (Optica Publishing Group, 2022), paper EF3A.5, DOI: 10.1364/EUVXRAY.2022.EF3A.5.

6. Hayk L. Gevorgyan, Andon A. Rangelov and Nikolay V. Vitanov, "**Broadband composite nonreciprocal polarization wave plates and optical isolators**", arXiv:2305.06431 [physics.optics], DOI: 10.48550/arXiv.2305.06431, submitted for publication

A.2 PRESENTATIONS

1. H. L. Gevorgyan, N. V. Vitanov, "**High-Fidelity Composite Rotation Gates**", Control of Quantum Dynamics of Atoms, Molecules, and Ensembles by Light, **CAMEL-XV**, June 2019, Nessebar, Bulgaria.

2. H. L. Gevorgyan, N. V. Vitanov, "**Ultrahigh-Fidelity Composite Rotation Gates**", Gordon Research Conference "Quantum Control of Light and Matter", **GRC**, August 2019, Salve Regina University, New Port, RI, USA.

3. H. L. Gevorgyan, N. V. Vitanov, "**Ultrahigh-Fidelity Composite Rotation Gates**", MSCA-ITN: Light-Matter Interfaces for Quantum Enhanced Technologies, **LIMQUET-2019**, September 2019, Nessebar, Bulgaria.

4. H. L. Gevorgyan, N. V. Vitanov, "**Composite pulses for ultrahigh-precision applications: quantum computing and more**", MSCA-ITN: Light-Matter Interfaces for Quantum Enhanced Technologies, **LIMQUET-2021**, September 2021, Oxford, UK.

5. H. L. Gevorgyan, N. V. Vitanov, "**Ultrabroadband (bat) and ultranarrowband (snake) composite π pulses**", The 9^{th} International Symposium "Optics & its applications 2022", **Optics-2022**, January 2022, Yerevan – Ashtarak, Armenia.

6. H. L. Gevorgyan, N. V. Vitanov, "**Ultrahigh-fidelity robust composite quantum phase gates**", The 9^{th} International Symposium "Optics & its applications 2022", **Optics-2022**, January 2022, Yerevan – Ashtarak, Armenia.

7. H. L. Gevorgyan, N. V. Vitanov, "**Ultrabroadband and Ultranarrowband Composite Polarization Half-Waveplates**", High-Brightness Sources and Light-Driven Interactions Congress, **OPTICA**, March 2022, Budapest, Hungary.

BIBLIOGRAPHY

[1] C. D. West and A. S. Makas, 'The spectral dispersion of birefringence, especially of birefringent plastic sheets', *Journal of the Optical Society of America*, vol. 39, no. 9, pp. 791–794, 1949. DOI: https://doi.org/10.1364/JOSA.39.000791.

[2] M. G. Destriau and J. Prouteau, 'Réalisation d'un quart d'onde quasi achromatique par juxtaposition de deux lames cristallines de même nature', *Le Journal de Physique et le Radium*, vol. 10, no. 2, pp. 53–55, 1949. DOI: https://doi.org/10.1051/jphysrad:0194900100205300.

[3] S. Pancharatnam, 'Achromatic combinations of birefringent plates. Part i: An achromatic circular polarizer', *Proceedings of the Indian Academy of Sciences, Section A*, vol. 41, no. 4, pp. 130–136, 1955. [Online]. Available: https://doi.org/10.1007/bf03047097.

[4] S. Pancharatnam, 'Achromatic combinations of birefringent plates. Part ii: An achromatic quarter-wp', *Proceedings of the Indian Academy of Sciences*, vol. 41, no. 4, pp. 137–144, 1955. [Online]. Available: https://doi.org/10.1007/BF03047098.

[5] S. E. Harris, E. O. Ammann and I. C. Chang, 'Optical network synthesis using birefringent crystals. i. Synthesis of lossless networks of equal-length crystals', *Journal of the Optical Society of America*, vol. 54, no. 10, pp. 1267–1279, 1964. DOI: https://doi.org/10.1364/JOSA.54.001267.

[6] C. M. McIntyre and S. E. Harris, 'Achromatic wave plates for the visible spectrum', *Journal of the Optical Society of America*, vol. 58, no. 12, pp. 1575–1580, 1968. DOI: https://doi.org/10.1364/JOSA.58.001575.

[7] T. Peters, S. S. Ivanov, D. Englisch, A. A. Rangelov, N. V. Vitanov and T. Halfmann, 'Variable ultrabroadband and narrowband composite polarization retarders', *Applied Optics*, vol. 51, no. 31, pp. 7466–7474, 2012. DOI: https://doi.org/10.1364/AO.51.007466.

[8] S. S. Ivanov, A. A. Rangelov, N. V. Vitanov, T. Peters and T. Halfmann, 'Highly efficient broadband conversion of light polarization by composite retarders', *Journal of the Optical Society of America A*, vol. 29, no. 3, pp. 265–269, 2012. DOI: https://doi.org/10.1364/JOSAA.29.000265.

[9] E. S. Dimova, S. S. Ivanov, G. S. Popkirov and N. V. Vitanov, 'Highly efficient broadband polarization retarders and tunable polarization filters made of composite stacks of ordinary wave plates', *Journal of the Optical Society of America A*, vol. 31, no. 5, pp. 952–956, 2014. DOI: https://doi.org/10.1364/JOSAA.31.000952.

[10] B. W. Shore, A. Rangelov, N. V. Vitanov and K. Bergmann, 'Piecewise adiabatic passage in polarization optics: An achromatic polarization rotator', *Advances in Chemical Physics*, vol. 159, pp. 219–234, 2016. DOI: https://doi.org/10.1002/9781119096276.ch5.

[11] S. Gulde, M. Riebe, G. P. T. Lancaster, C. Becher, J. Eschner, H. Häffner, F. Schmidt-Kaler, I. L. Chuang and R. Blatt, 'Implementation of the Deutsch–Jozsa algorithm on an ion-trap quantum computer', *Nature (London)*, vol. 421, no. 6918, pp. 48–50, 2003. DOI: https://doi.org/10.1038/nature01336.

[12] F. Schmidt-Kaler, H. Häffner, M. Riebe, S. Gulde, G. P. T. Lancaster, T. Deuschle, C. Becher, C. F. Roos, J. Eschner and R. Blatt, 'Realization of the Cirac–Zoller controlled-NOT quantum gate', *Nature (London)*, vol. 422, no. 6930, pp. 408–411, 2003. DOI: https://doi.org/10.1038/nature01494.

[13] H. Häffner, C. F. Roos and R. Blatt, 'Quantum computing with trapped ions', *Physics Reports*, vol. 469, no. 4, pp. 155–203, 2008. DOI: https://doi.org/10.1016/j.physrep.2008.09.003.

[14] N. Timoney, V. Elman, S. Glaser, C. Weiss, M. Johanning, W. Neuhauser and C. Wunderlich, 'Error-resistant single-qubit gates with trapped ions', *Physical Review A*, vol. 77, no. 5, pp. 052334, 1–7, 2008. DOI: https://doi.org/10.1103/PhysRevA.77.052334.

[15] T. Monz, K. Kim, W. Hänsel, M. Riebe, A. S. Villar, P. Schindler, M. Chwalla, M. Hennrich and R. Blatt, 'Realization of the quantum Toffoli gate with trapped ions', *Physical Review Letters*, vol. 102, no. 4, pp. 040501, 1–4, 2009. DOI: https://doi.org/10.1103/PhysRevLett.102.040501.

[16] G. Zarantonello, H. Hahn, J. Morgner, M. Schulte, A. Bautista-Salvador, R. F. Werner, K. Hammerer and C. Ospelkaus, 'Robust and resource-efficient microwave near-field entangling $_9Be^+$ gate', *Physical Review Letters*, vol. 123, no. 26, pp. 260503, 1–6, 2019. DOI: https://doi.org/10.1103/PhysRevLett.123.260503.

[17] C. M. Shappert, J. T. Merrill, K. R. Brown, J. M. Amini, C. Volin, S. C. Doret, H. Hayden, C.-S. Pai, K. R. Brown and A. W. Harter, 'Spatially uniform single-qubit gate operations with near-field microwaves and composite pulse compensation', *New Journal of Physics*, vol. 15, no. 8, pp. 083053, 1–12, 2013. DOI: https://doi.org/10.1088/1367-2630/15/8/083053.

[18] E. Mount, C. Kabytayev, S. Crain, R. Harper, S.-Y. Baek, G. Vrijsen, S. T. Flammia, K. R. Brown, P. Maunz and J. Kim, 'Error compensation of single-qubit gates in a surface-electrode ion trap using composite pulses', *Physical Review A*, vol. 92, no. 6, pp. 060301, 1–5, 2015. DOI: https://doi.org/10.1103/PhysRevA.92.060301.

[19] W. Rakreungdet, J. H. Lee, K. F. Lee, B. E. Mischuck, E. Montano and P. S. Jessen, 'Accurate microwave control and real-time diagnostics of neutral-atom qubits', *Physical Review A*, vol. 79, no. 2, pp. 022316, 1–9, 2009. DOI: https://doi.org/10.1103/PhysRevA.79.022316.

[20] D. Schraft, T. Halfmann, G. T. Genov and N. V. Vitanov, 'Experimental demonstration of composite adiabatic passage', *Physical Review A*, vol. 88, no. 6, pp. 063406, 1–9, 2013. DOI: https://doi.org/10.1103/PhysRevA.88.063406.

[21] G. T. Genov, D. Schraft, N. V. Vitanov and T. Halfmann, 'Arbitrarily accurate pulse sequences for robust dynamical decoupling', *Physical Review Letters*, vol. 118, no. 3, pp. 133202, 1–5, 2017. DOI: https://doi.org/10.1103/PhysRevLett.118.133202.

[22] A. Bruns, G. T. Genov, M. Hain, N. V. Vitanov and T. Halfmann, 'Experimental demonstration of composite stimulated Raman adiabatic passage', *Physical Review A*, vol. 98, no. 5, pp. 053413, 1–10, 2018. DOI: https://doi.org/10.1103/PhysRevA.98.053413.

[23] X. Wang, L. S. Bishop, J. P. Kestner, E. Barnes, K. Sun and S. D. Sarma, 'Composite pulses for robust universal control of singlet–triplet qubits', *Nature Communications*, vol. 3, pp. 997, 1–7, 2012. DOI: https://doi.org/10.1038/ncomms2003.

[24] J. P. Kestner, X. Wang, L. S. Bishop, E. Barnes and S. D. Sarma, 'Noise-resistant control for a spin qubit array', *Physical Review Letters*, vol. 110, no. 14, pp. 140502, 1–5, 2013. DOI: https://doi.org/10.1103/PhysRevLett.110.140502.

[25] X. Wang, L. S. Bishop, E. Barnes, J. P. Kestner and S. D. Sarma, 'Robust quantum gates for singlet-triplet spin qubits using composite pulses', *Physical Review A*, vol. 89, no. 2, pp. 022310, 1–20, 2014. DOI: https://doi.org/10.1103/PhysRevA.89.022310.

[26] C. Zhang, R. E. Throckmorton, X.-C. Yang, X. Wang, E. Barnes and S. D. Sarma, 'Randomized benchmarking of barrier versus tilt control of a singlet-triplet qubit', *Physical Review Letters*, vol. 118, no. 21, pp. 216802, 1–6, 2017. DOI: https://doi.org/10.1103/PhysRevLett.118.216802.

[27] G. T. Hickman, X. Wang, J. P. Kestner and S. D. Sarma, 'Dynamically corrected gates for an exchange-only qubit', *Physical Review B*, vol. 88, no. 16, pp. 161303, 1–5, 2013. DOI: https://doi.org/10.1103/PhysRevB.88.161303.

[28] K. Eng *et al.*, 'Isotopically enhanced triple-quantum-dot qubit', *Science Advances*, vol. 1, no. 4, e1500214, 1–7, 2015. DOI: https://doi.org/10.1126/sciadv.1500214.

[29] X. Rong, J. Geng, F. Shi, Y. Liu, K. Xu, W. Ma, F. Kong, Z. Jiang, Y. Wu and J. Du, 'Experimental fault-tolerant universal quantum gates with solid-state spins under ambient conditions', *Nature Communications*, vol. 6, pp. 8748, 1–7, 2015. DOI: https://doi.org/10.1038/ncomms9748.

[30] T. Zanon-Willette, R. Lefevre, R. Metzdorff, N. Sillitoe, S. Almonacil, M. Minissale, E. de Clercq, A. V. Taichenachev, V. I. Yudin and E. Arimondo, 'Composite laser-pulses spectroscopy for high-accuracy optical clocks: A review of recent progress and perspectives', *Reports on Progress in Physics*, vol. 81, pp. 094401, 1–35, 2018. DOI: https://doi.org/10.1088/1361-6633/aac9e9.

[31] D. L. Butts, K. Kotru, J. M. Kinast, A. M. Radojevic, B. P. Timmons and R. E. Stoner, 'Efficient broadband Raman pulses for large-area atom interferometry', *Journal of the Optical Society of America B*, vol. 30, no. 4, pp. 922–927, 2013. DOI: https://doi.org/10.1364/JOSAB.30.000922.

[32] A. Dunning, R. Gregory, J. Bateman, N. Cooper, M. Himsworth, J. A. Jones and T. Freegarde, 'Composite pulses for interferometry in a thermal cold atom cloud', *Physical Review A*, vol. 90, no. 3, pp. 033608, 1–10, 2014. DOI: https://doi.org/10.1103/PhysRevA.90.033608.

[33] P. Berg, S. Abend, G. Tackmann, C. Schubert, E. Giese, W. P. Schleich, F. A. Narducci, W. Ertmer and E. M. Rasel, 'Composite-light-pulse technique for high-precision atom interferometry', *Physical Review Letters*, vol. 114, no. 6, pp. 063002, 1–5, 2015. DOI: https://doi.org/10.1103/PhysRevLett.114.063002.

[34] G. Demeter, 'Composite pulses for high-fidelity population inversion in optically dense, inhomogeneously broadened atomic ensembles', *Physical Review A*, vol. 93, no. 2, pp. 023830, 1–8, 2016. DOI: https://doi.org/10.1103/PhysRevA.93.023830.

[35] C. D. Aiello, M. Hirose and P. Cappellaro, 'Composite-pulse magnetometry with a solid-state quantum sensor', *Nature Communications*, vol. 4, pp. 1419, 1–6, 2013. DOI: https://doi.org/10.1038/ncomms2375.

[36] C. Ventura-Velázquez, B. J. Ávila, E. Kyoseva and B. M. Rodrǵuez-Lara, 'Robust optomechanical state transfer under composite phase driving', *Scientific Reports*, vol. 9, no. 1, pp. 4382, 1–10, 2019. DOI: https://doi.org/10.1038/s41598-019-40492-y.

[37] S. Wimperis, 'Broadband, narrowband, and passband composite pulses for use in advanced NMR experiments', *Journal of Magnetic Resonance, Series A*, vol. 109, no. 2, pp. 221–231, 1994. DOI: https://doi.org/10.1006/jmra.1994.1159.

[38] H. K. Cummins, G. Llewellyn and J. A. Jones, 'Tackling systematic errors in quantum logic gates with composite rotations', *Physical Review A*, vol. 67, no. 4, pp. 042308, 1–6, 2003. DOI: https://doi.org/10.1103/PhysRevA.67.042308.

[39] R. Tycko, H. M. Cho, E. Schneider and A. Pines, 'Composite pulses without phase distortion', *Journal of Magnetic Resonance*, vol. 61, no. 1, pp. 90–101, 1985. DOI: https://doi.org/10.1016/0022-2364(85)90270-7.

[40] M. H. Levitt, 'Composite pulses', *Progress in Nuclear Magnetic Resonance Spectroscopy*, vol. 18, no. 2, pp. 61–122, 1986. DOI: https://doi.org/10.1016/0079-6565(86)80005-x.

[41] M. H. Levitt, 'Composite pulses', *Encyclopedia of Magnetic Resonance*, pp. 1–16, 2007. DOI: https://doi.org/10.1002/9780470034590.emrstm0086.

[42] J. T. Merrill and K. R. Brown, 'Progress in compensating pulse sequences for quantum computation', *Advances in Chemical Physics: Quantum Information and Computation for Chemistry*, vol. 154, pp. 241–294, 2014. DOI: https://doi.org/10.1002/9781118742631.ch10.

[43] H. L. Gevorgyan and N. V. Vitanov, 'Ultrahigh-fidelity composite rotational quantum gates', *Physical Review A*, vol. 104, no. 1, pp. 012609, 1–12, 2021. DOI: https://doi.org/10.1103/PhysRevA.104.012609.

[44] K. R. Brown, A. W. Harrow and I. L. Chuang, 'Arbitrarily accurate composite pulse sequences', *Physical Review A*, vol. 70, no. 5, pp. 052318, 1–4, 2004. DOI: https://doi.org/10.1103/PhysRevA.70.052318.

[45] T. Ichikawa, M. Bando, Y. Kondo and M. Nakahara, 'Geometric aspects of composite pulses', *Philosophical Transactions of The Royal Society A*, vol. 370, no. 1976, pp. 4671–4689, 2012. DOI: https://doi.org/10.1098/rsta.2011.0358.

[46] H. L. Gevorgyan and N. V. Vitanov, 'Ultrahigh-fidelity composite quantum phase gates', *arXiv:2306.10340 [quant-ph]*, 2023. DOI: https://doi.org/10.48550/arXiv.2306.10340.

[47] H. L. Gevorgyan, 'Ultrabroadband and ultranarrowband composite polarization half-waveplates', in *Compact EUV & X-ray Light Sources, Optica High-brightness Sources and Light-driven Interactions Congress*, Technical Digest Series (Optica Publishing Group), 2022, EF3A–5, 1–2. DOI: https://doi.org/10.1364/EUVXRAY.2022.EF3A.5.

[48] H. L. Gevorgyan, A. A. Rangelov and N. V. Vitanov, 'Broadband composite nonreciprocal polarization wave plates and optical isolators', *arXiv:2305.06431 [physics.optics]*, 2023. DOI: https://doi.org/10.48550/arXiv.2305.06431.

[49] N. V. Vitanov, T. Halfmann, B. W. Shore and K. Bergmann, 'Laser-induced population transfer by adiabatic passage techniques', *Annual Review of Physical Chemistry*, vol. 52, no. 1, pp. 763–809, 2001. DOI: https://10.1146/annurev.physchem.52.1.763.

[50] L. D. Landau, 'Zur theorie der energieubertragung ii', *Physikalische Zeitschrift der Sowjetunion*, vol. 2, pp. 46–51, 1932.

[51] E. Majorana, 'Atomi orientati in campo magnetico variabile', *Il Nuovo Cimento (1924-1942)*, vol. 9, no. 2, pp. 43–50, 1932. DOI: https://doi.org/10.1007/BF02960953.

[52] E. C. G. Stückelberg, 'Theorie der unelastischen Stösse zwischen Atomen', *Helvetica Physica Acta*, vol. 5, p. 369, 1932.

[53] C. Zener, 'Non-adiabatic crossing of energy levels', *Proceedings of the Royal Society A: Mathematical, Physical and Engineering Sciences*, vol. 137, no. 833, pp. 696–702, 1932. DOI: https://10.1098/rspa.1932.0165.

[54] L. P. Yatsenko, N. V. Vitanov, B. W. Shore, T. Rickes and K. Bergmann, 'Creation of coherent superpositions using Stark-chirped rapid adiabatic passage', *Optics Communications*, vol. 204, no. 1-6, pp. 413–423, 2002. DOI: https://doi.org/10.1016/S0030-4018(02)01303-2.

[55] N. V. Vitanov and B. W. Shore, 'Stimulated Raman adiabatic passage in a two-state system', *Physical Review A*, vol. 73, no. 5, pp. 053402, 1–4, 2006. DOI: https://10.1103/physreva.73.053402.

[56] R. Yamazaki, K.-i. Kanda, F. Inoue, K. Toyoda and S. Urabe, 'Robust generation of superposition states', *Physical Review A*, vol. 78, no. 2, pp. 023808, 1–6, 2008. DOI: https://10.1103/physreva.78.023808.

[57] K. N. Zlatanov and N. V. Vitanov, 'Adiabatic generation of arbitrary coherent superpositions of two quantum states: Exact and approximate solutions', *Physical Review A*, vol. 96, no. 1, pp. 013415, 1–10, 2017. DOI: https://10.1103/physreva.96.013415.

[58] J. Randall, A. M. Lawrence, S. C. Webster, S. Weidt, N. V. Vitanov and W. K. Hensinger, 'Generation of high-fidelity quantum control methods for multilevel systems', *Physical Review A*, vol. 98, no. 4, pp. 043414, 1–9, 2018. DOI: https://10.1103/physreva.98.043414.

[59] N. V. Vitanov, A. A. Rangelov, B. W. Shore and K. Bergmann, 'Stimulated Raman adiabatic passage in physics, chemistry, and beyond', *Reviews of Modern Physics*, vol. 89, no. 1, pp. 015006, 1–66, 2017. DOI: https://10.1103/revmodphys.89.015006.

[60] K. N. Zlatanov and N. V. Vitanov, 'Generation of arbitrary qubit states by adiabatic evolution split by a phase jump', *Physical Review A*, vol. 101, no. 1, pp. 013426, 1–9, 2020. DOI: https://10.1103/physreva.101.013426.

[61] P. Marte, P. Zoller and J. L. Hall, 'Coherent atomic mirrors and beam splitters by adiabatic passage in multilevel systems', *Physical Review A*, vol. 44, no. 7, R4118–R4121, 1991. DOI: https://10.1103/physreva.44.r4118.

[62] M. Weitz, B. C. Young and S. Chu, 'Atomic interferometer based on adiabatic population transfer', *Physical Review Letters*, vol. 73, no. 19, pp. 2563–2566, 1994. DOI: https://doi.org/10.1103/PhysRevLett.73.2563.

[63] N. V. Vitanov, K. A. Suominen and B. W. Shore, 'Creation of coherent atomic superpositions by fractional stimulated Raman adiabatic passage', *Journal of Physics B: Atomic, Molecular and Optical Physics*, vol. 32, no. 18, pp. 4535–4546, 1999. DOI: https://10.1088/0953-4075/32/18/312.

[64] R. Unanyan, M. Fleischhauer, B. W. Shore and K. Bergmann, 'Robust creation and phase-sensitive probing of superposition states via stimulated Raman adiabatic passage (STIRAP) with degenerate dark states', *Optics Communications*, vol. 155, no. 1-3, pp. 144–154, 1998. DOI: https://doi.org/10.1016/S0030-4018(98)00358-7.

[65] H. Theuer, R. G. Unanyan, C. Habscheid, K. Klein and K. Bergmann, 'Novel laser controlled variable matter wave beamsplitter', *Optics Express*, vol. 4, no. 2, pp. 77–83, 1999. DOI: https://doi.org/10.1364/oe.4.000077.

[66] F. Vewinger, M. Heinz, R. G. Fernandez, N. V. Vitanov and K. Bergmann, 'Creation and measurement of a coherent superposition of quantum states', *Physical Review Letters*, vol. 91, no. 21, pp. 213001, 1–4, 2003. DOI: https://doi.org/10.1103/physrevlett.91.213001.

[67] P. A. Ivanov, B. T. Torosov and N. V. Vitanov, 'Navigation between quantum states by quantum mirrors', *Physical Review A*, vol. 75, no. 1, pp. 012323, 1–9, 2007. DOI: https://10.1103/physreva.75.012323.

[68] B. Rousseaux, S. Guérin and N. V. Vitanov, 'Arbitrary qudit gates by adiabatic passage', *Physical Review A*, vol. 87, no. 3, pp. 032328, 1–4, 2013. DOI: https://10.1103/physreva.87.032328.

[69] M. H. Levitt and R. Freeman, 'NMR population inversion using a composite pulse', *Journal of Magnetic Resonance (1969)*, vol. 33, no. 2, pp. 473–476, 1979. DOI: https://10.1016/0022-2364(79)90265-8.

[70] R. Freeman, S. P. Kempsell and M. H. Levitt, 'Radiofrequency pulse sequences which compensate their own imperfections', *Journal of Magnetic Resonance (1969)*, vol. 38, no. 3, pp. 453–479, 1980. DOI: https://10.1016/0022-2364(80)90327-3.

[71] M. H. Levitt, 'Symmetrical composite pulse sequences for NMR population inversion. i. Compensation of radiofrequency field inhomogeneity', *Journal of Magnetic Resonance (1969)*, vol. 48, no. 2, pp. 234–264, 1982. DOI: https://doi.org/10.1016/0022-2364(82)90275-X.

[72] M. H. Levitt and R. R. Ernst, 'Composite pulses constructed by a recursive expansion procedure', *Journal of Magnetic Resonance (1969)*, vol. 55, no. 2, pp. 247–254, 1983. DOI: https://doi.org/10.1016/0022-2364(83)90236-6.

[73] S. Wimperis, 'Broadband and narrowband composite excitation sequences', *Journal of Magnetic Resonance (1969)*, vol. 86, no. 1, pp. 46–59, 1990. DOI: https://doi.org/10.1016/0022-2364(90)90210-z.

[74] S. Wimperis, 'Iterative schemes for phase-distortionless composite 180° pulses', *Journal of Magnetic Resonance (1969)*, vol. 93, no. 1, pp. 199–206, 1991. DOI: https://doi.org/10.1016/0022-2364(91)90043-s.

[75] B. T. Torosov and N. V. Vitanov, 'Smooth composite pulses for high-fidelity quantum information processing', *Physical Review A*, vol. 83, no. 5, pp. 053420, 1–7, 2011. DOI: https://doi.org/10.1103/physreva.83.053420.

[76] B. T. Torosov, S. Guérin and N. V. Vitanov, 'High-fidelity adiabatic passage by composite sequences of chirped pulses', *Physical Review Letters*, vol. 106, no. 23, pp. 233001, 1–4, 2011. DOI: https://doi.org/10.1103/PhysRevLett.106.233001.

[77] G. T. Genov, D. Schraft, T. Halfmann and N. V. Vitanov, 'Correction of arbitrary field errors in population inversion of quantum systems by universal composite pulses', *Physical Review Letters*, vol. 113, no. 4, pp. 043001, 1–5, 2014. DOI: https://doi.org/10.1103/physrevlett.113.043001.

[78] R. Tycko and A. Pines, 'Iterative schemes for broad-band and narrow-band population inversion in NMR', *Chemical Physics Letters*, vol. 111, no. 4-5, pp. 462–467, 1984. DOI: https://doi.org/10.1016/0009-2614(84)85541-4.

[79] R. Tycko, A. Pines and J. Guckenheimer, 'Fixed point theory of iterative excitation schemes in NMR', *The Journal of Chemical Physics*, vol. 83, no. 6, pp. 2775–2802, 1985. DOI: https://doi.org/10.1063/1.449228.

[80] A. J. Shaka and R. Freeman, 'Spatially selective radiofrequency pulses', *Journal of Magnetic Resonance (1969)*, vol. 59, no. 1, pp. 169–176, 1984. DOI: https://doi.org/10.1016/0022-2364(84)90297-x.

[81] N. V. Vitanov, 'Arbitrarily accurate narrowband composite pulse sequences', *Physical Review A*, vol. 84, no. 6, pp. 065404, 1–4, 2011. DOI: https://doi.org/10.1103/physreva.84.065404.

[82] S. S. Ivanov and N. V. Vitanov, 'High-fidelity local addressing of trapped ions and atoms by composite sequences of laser pulses', *Optics Letters*, vol. 36, no. 7, pp. 1275–1277, 2011. DOI: https://doi.org/10.1364/ol.36.001275.

[83] B. T. Torosov, S. S. Ivanov and N. V. Vitanov, 'Narrowband and passband composite pulses for variable rotations', *Physical Review A*, vol. 102, no. 1, pp. 013105, 1–6, 2020. DOI: https://doi.org/10.1103/physreva.102.013105.

[84] H. M. Cho, R. Tycko, A. Pines and J. Guckenheimer, 'Iterative maps for bistable excitation of two-level systems', *Physical Review Letters*, vol. 56, no. 18, pp. 1905–1908, 1986. DOI: https://doi.org/10.1103/PhysRevLett.56.1905.

[85] H Cho, J. Baum and A. Pines, 'Iterative maps with multiple fixed points for excitation of two level systems', *The Journal of Chemical Physics*, vol. 86, no. 6, pp. 3089–3106, 1987. DOI: https://doi.org/10.1063/1.452020.

[86] S. Wimperis, 'Composite pulses with rectangular excitation and inversion profiles', *Journal of Magnetic Resonance (1969)*, vol. 83, no. 3, pp. 509–524, 1989. DOI: https://doi.org/10.1016/0022-2364(89)90346-6.

[87] E. Kyoseva and N. V. Vitanov, 'Arbitrarily accurate passband composite pulses for dynamical suppression of amplitude noise', *Physical Review A*, vol. 88, no. 6, pp. 063410, 1–7, 2013. DOI: https://doi.org/10.1103/PhysRevA.88.063410.

[88] J. A. Jones, 'Designing short robust NOT gates for quantum computation', *Physical Review A*, vol. 87, no. 5, pp. 052317, 1–11, 2013. DOI: https://doi.org/10.1103/physreva.87.052317.

[89] J. A. Jones, 'Nested composite NOT gates for quantum computation', *Physics Letters A*, vol. 377, no. 40, pp. 2860–2862, 2013. DOI: https://doi.org/10.1016/j.physleta.2013.08.040.

[90] S. Husain, M. Kawamura and J. A. Jones, 'Further analysis of some symmetric and antisymmetric composite pulses for tackling pulse strength errors', *Journal of Magnetic Resonance*, vol. 230, pp. 145–154, 2013. DOI: https://doi.org/10.1016/j.jmr.2013.02.007.

[91] B. T. Torosov and N. V. Vitanov, 'High-fidelity error-resilient composite phase gates', *Physical Review A*, vol. 90, no. 1, pp. 012341, 1–5, 2014. DOI: https://doi.org/10.1103/physreva.90.012341.

[92] J. A. Jones, 'Robust Ising gates for practical quantum computation', *Physical Review A*, vol. 67, no. 1, pp. 012317, 1–3, 2003. DOI: https://doi.org/10.1103/physreva.67.012317.

[93] J. A. Jones, 'Suppressing weak Ising couplings: Tailored gates for quantum computation', *Physics Letters A*, vol. 316, no. 1-2, pp. 24–28, 2003. DOI: https://doi.org/10.1016/s0375-9601(03)01130-7.

[94] L. Xiao and J. A. Jones, 'Robust logic gates and realistic quantum computation', *Physical Review A*, vol. 73, no. 3, pp. 032334, 1–5, 2006. DOI: https://doi.org/10.1103/physreva.73.032334.

[95] W. G. Alway and J. A. Jones, 'Arbitrary precision composite pulses for NMR quantum computing', *Journal of Magnetic Resonance*, vol. 189, no. 1, pp. 114–120, 2007. DOI: https://doi.org/10.1016/j.jmr.2007.09.001.

[96] C. D. Hill, 'Robust controlled-NOT gates from almost any interaction', *Physical Review Letters*, vol. 98, no. 18, pp. 180501, 1–4, 2007. DOI: https://doi.org/10.1103/PhysRevLett.98.180501.

[97] M. J. Testolin, C. D. Hill, C. J. Wellard and L. C. L. Hollenberg, 'Robust controlled-NOT gate in the presence of large fabrication-induced variations of the exchange interaction strength', *Physical Review A*, vol. 76, no. 1, pp. 012302, 1–8, 2007. DOI: https://doi.org/10.1103/PhysRevA.76.012302.

[98] S. S. Ivanov and N. V. Vitanov, 'Composite two-qubit gates', *Physical Review A*, vol. 92, no. 2, pp. 022333, 1–8, 2015. DOI: https://doi.org/10.1103/PhysRevA.92.022333.

[99] S. S. Ivanov and N. V. Vitanov, 'Scalable uniform construction of highly conditional quantum gates', *Physical Review A*, vol. 84, no. 2, pp. 022319, 1–5, 2011. DOI: https://doi.org/10.1103/physreva.84.022319.

[100] J. A. Jones, 'Quantum computing with NMR', *Progress in Nuclear Magnetic Resonance Spectroscopy*, vol. 59, no. 2, pp. 91–120, 2011. DOI: https://doi.org/10.1016/j.pnmrs.2010.11.001.

[101] B. T. Torosov and N. V. Vitanov, 'Composite pulses with errant phases', *Physical Review A*, vol. 100, no. 2, pp. 023410, 1–9, 2019. DOI: https://doi.org/10.1103/PhysRevA.100.023410.

[102] M. A. Nielsen and I. L. Chuang, *Quantum Computation and Quantum Information*. Cambridge University Press, 2000.

[103] L. M. K. Vandersypen and I. L. Chuang, 'NMR techniques for quantum control and computation', *Reviews of Modern Physics*, vol. 76, no. 4, pp. 1037–1069, 2005. DOI: https://10.1103/revmodphys.76.1037.

[104] A. Abraham, *The Principles of Nuclear Magnetism*. Clarendon, Oxford, 1961.

[105] R. Freeman, *Spin choreography: Basic steps in high resolution nmr*, 1997.

[106] R. S. Said and J. Twamley, 'Robust control of entanglement in a nitrogen-vacancy center coupled to a ^{13}C nuclear spin in diamond', *Physical Review A*, vol. 80, no. 3, pp. 032303, 1–7, 2009. DOI: https://doi.org/10.1103/physreva.80.032303.

[107] E. Collin, G. Ithier, A. Aassime, P. Joyez, D. Vion and D. Esteve, 'NMR-like control of a quantum bit superconducting circuit', *Physical Review Letters*, vol. 93, no. 15, pp. 157005, 1–4, 2004. DOI: https://doi.org/10.1103/PhysRevLett.93.157005.

[108] C. M. Collins, Z. Wang, W. Mao, J. Fang, W. Liu and M. B. Smith, 'Array-optimized composite pulse for excellent whole-brain homogeneity in high-field MRI', *Magnetic Resonance in Medicine*, vol. 57, no. 3, pp. 470–474, 2007. DOI: https://doi.org/10.1002/mrm.21172.

[109] H. K. Cummins and J. A. Jones, 'Use of composite rotations to correct systematic errors in NMR quantum computation', *New Journal of Physics*, vol. 2, no. 1, 6.1–6.12, 2000. DOI: https://doi.org/10.1088/1367-2630/2/1/006.

[110] M. Riebe, H. Häffner, C. F. Roos, W. Hänsel, J. Benhelm, G. P. T. Lancaster, T. W. Körber, C. Becher, F. Schmidt-Kaler, D. F. V. James *et al.*, 'Deterministic quantum teleportation with atoms', *Nature*, vol. 429, no. 6993, pp. 734–737, 2004. DOI: https://doi.org/10.1038/nature02570.

[111] M. D. Barrett, J. Chiaverini, T. Schaetz, J. Britton, W. M. Itano, J. D. Jost, E. Knill, C. Langer, D. Leibfried, R. Ozeri *et al.*, 'Deterministic quantum teleportation of atomic qubits', *Nature*, vol. 429, no. 6993, pp. 737–739, 2004. DOI: https://doi.org/10.1038/nature02608.

[112] N. F. Scherer, R. J. Carlson, A. Matro, M. Du, A. J. Ruggiero, V. Romero-Rochin, J. A. Cina, G. R. Fleming and S. A. Rice, 'Fluorescence-detected wave packet interferometry: Time resolved molecular spectroscopy with sequences of femtosecond phase-locked pulses', *The Journal of Chemical Physics*, vol. 95, no. 3, pp. 1487–1511, 1991. DOI: https://doi.org/10.1063/1.461064.

[113] X.-C. Yang, M.-H. Yung and X. Wang, 'Neural-network-designed pulse sequences for robust control of singlet-triplet qubits', *Physical Review A*, vol. 97, no. 4, pp. 042324, 1–9, 2018. DOI: https://doi.org/10.1103/PhysRevA.97.042324.

[114] M. Bando, T. Ichikawa, Y. Kondo, N. Nemoto, M. Nakahara and Y. Shikano, 'Concatenated composite pulses applied to liquid-state nuclear magnetic resonance spectroscopy', *Scientific Reports*, vol. 10, no. 1, pp. 2126, 1–10, 2020. DOI: https://doi.org/10.1038/s41598-020-58823-9.

[115] A. A. Rangelov and E. Kyoseva, 'Broadband composite polarization rotator', *Optics Communications*, vol. 338, pp. 574–577, 2015. DOI: https://doi.org/10.1016/j.optcom.2014.11.037.

[116] B. W. Shore, *The Theory of Coherent Atomic Excitation*. Wiley, 1990.

[117] B. W. Shore, *Manipulating Quantum Structures Using Laser Pulses*. Cambridge University Press, 2011.

[118] D. Guéry-Odelin, A. Ruschhaupt, A. Kiely, E. Torrontegui, S. Martínez-Garaot and J. G. Muga, 'Shortcuts to adiabaticity: Concepts, methods, and applications', *Reviews of Modern Physics*, vol. 91, no. 4, pp. 045001, 1–54, 2019. DOI: https://doi.org/10.1103/revmodphys.91.045001.

[119] L.-M. Duan, M. D. Lukin, J. I. Cirac and P. Zoller, 'Long-distance quantum communication with atomic ensembles and linear optics', *Nature*, vol. 414, no. 6862, pp. 413–418, 2001. DOI: https://doi.org/10.1038/35106500.

[120] A. I. Lvovsky, B. C. Sanders and W. Tittel, 'Optical quantum memory', *Nature Photonics*, vol. 3, no. 12, pp. 706–714, 2009. DOI: https://doi.org/10.1038/nphoton.2009.231.

[121] N. Sangouard, C. Simon, H. de Riedmatten and N. Gisin, 'Quantum repeaters based on atomic ensembles and linear optics', *Reviews of Modern Physics*, vol. 83, no. 1, pp. 33–80, 2011. DOI: https://doi.org/10.1103/revmodphys.83.33.

[122] S.-J. Yang, X.-J. Wang, X.-H. Bao and J.-W. Pan, 'An efficient quantum light–matter interface with sub-second lifetime', *Nature Photonics*, vol. 10, no. 6, 381–384, 2016. DOI: https://doi.org/10.1038/nphoton.2016.51.

[123] Y.-F. Pu, N. Jiang, W. Chang, H.-X. Yang, C. Li and L.-M. Duan, 'Experimental realization of a multiplexed quantum memory with 225 individually accessible memory cells', *Nature Communications*, vol. 8, pp. 15359, 1–6, 2017. DOI: https://doi.org/10.1038/ncomms15359.

[124] C. Laplane, P. Jobez, J. Etesse, N. Gisin and M. Afzelius, 'Multimode and long-lived quantum correlations between photons and spins in a crystal', *Physical Review Letters*, vol. 118, no. 21, pp. 210501, 1–5, 2017. DOI: https://doi.org/10.1103/physrevlett.118.210501.

[125] K. Kutluer, M. Mazzera and H. de Riedmatten, 'Solid-state source of nonclassical photon pairs with embedded multimode quantum memory', *Physical Review Letters*, vol. 118, no. 21, pp. 210502, 1–6, 2017. DOI: https://doi.org/10.1103/physrevlett.118.210502.

[126] N. Gisin and R. Thew, 'Quantum communication', *Nature Photonics*, vol. 1, no. 3, 165–171, 2007. DOI: https://doi.org/10.1038/nphoton.2007.22.

[127] R. Ursin *et al.*, 'Entanglement-based quantum communication over 144 km', *Nature Physics*, vol. 3, no. 7, 481–486, 2007. DOI: https://doi.org/10.1038/nphys629.

[128] H. J. Kimble, 'The quantum internet', *Nature*, vol. 453, no. 7198, pp. 1023–1030, 2008. DOI: https://doi.org/10.1038/nature07127.

[129] W. Zhang, D.-S. Ding, Y.-B. Sheng, L. Zhou, B.-S. Shi and G.-C. Guo, 'Quantum secure direct communication with quantum memory', *Physical Review Letters*, vol. 118, no. 22, pp. 220501, 1–6, 2017. DOI: https://doi.org/10.1103/physrevlett.118.220501.

[130] Y.-A. Chen *et al.*, 'An integrated space-to-ground quantum communication network over 4,600 kilometres', *Nature*, vol. 589, no. 7841, 214–219, 2021. DOI: https://doi.org/10.1038/s41586-020-03093-8.

[131] P. Kok, W. J. Munro, K. Nemoto, T. C. Ralph, J. P. Dowling and G. J. Milburn, 'Linear optical quantum computing with photonic qubits', *Reviews of Modern Physics*, vol. 79, no. 1, 135–174, 2007. DOI: https://doi.org/10.1103/revmodphys.79.135.

[132] S. Barz, 'Quantum computing with photons: Introduction to the circuit model, the one-way quantum computer, and the fundamental principles of photonic experiments', *Journal of Physics B: Atomic, Molecular and Optical Physics*, vol. 48, no. 8, pp. 083001, 1–25, 2015. DOI: https://doi.org/10.1088/0953-4075/48/8/083001.

[133] T. Rudolph, 'Why I am optimistic about the silicon-photonic route to quantum computing', *APL Photonics*, vol. 2, no. 3, pp. 030901, 1–19, 2017. DOI: https://doi.org/10.1063/1.4976737.

[134] S. Takeda and A. Furusawa, 'Toward large-scale fault-tolerant universal photonic quantum computing', *APL Photonics*, vol. 4, no. 6, pp. 060902, 1–13, 2019. DOI: https://doi.org/10.1063/1.5100160.

[135] R. H. Dicke, 'Coherence in spontaneous radiation processes', *Physical Review*, vol. 93, no. 1, 99–110, 1954. DOI: https://doi.org/10.1103/physrev.93.99.

[136] S. S. Ivanov, P. A. Ivanov and N. V. Vitanov, 'Simple implementation of a quantum search with trapped ions', *Physical Review A*, vol. 78, no. 3, pp. 030301, 1–4, 2008. DOI: https://doi.org/10.1103/physreva.78.030301.

[137] S. S. Ivanov, P. A. Ivanov, I. E. Linington and N. V. Vitanov, 'Scalable quantum search using trapped ions', *Physical Review A*, vol. 81, no. 4, pp. 042328, 1–6, 2010. DOI: https://doi.org/10.1103/physreva.81.042328.

[138] I. E. Linington, P. A. Ivanov and N. V. Vitanov, 'Quantum search in a nonclassical database of trapped ions', *Physical Review A*, vol. 79, no. 1, pp. 012322, 1–7, 2009. DOI: https://doi.org/10.1103/physreva.79.012322.

[139] G. Tóth, 'Detection of multipartite entanglement in the vicinity of symmetric Dicke states', *Journal of the Optical Society of America B*, vol. 24, no. 2, pp. 275–281, 2007. DOI: https://doi.org/10.1364/josab.24.000275.

[140] A. R. U. Devi, R. Prabhu and A. K. Rajagopal, 'Characterizing multiparticle entanglement in symmetric N-qubit states via negativity of covariance matrices', *Physical Review Letters*, vol. 98, no. 6, pp. 060501, 1–4, 2007. DOI: https://doi.org/10.1103/physrevlett.98.060501.

[141] J. K. Stockton, J. M. Geremia, A. C. Doherty and H. Mabuchi, 'Characterizing the entanglement of symmetric many-particle spin-$\frac{1}{2}$ systems', *Physical Review A*, vol. 67, no. 2, pp. 022112, 1–17, 2003. DOI: https://doi.org/10.1103/physreva.67.022112.

[142] M. Bourennane, M. Eibl, S. Gaertner, N. Kiesel, C. Kurtsiefer and H. Weinfurter, 'Entanglement persistency of multiphoton entangled states', *Physical Review Letters*, vol. 96, no. 10, pp. 100502, 1–4, 2006. DOI: https://doi.org/10.1103/physrevlett.96.100502.

[143] W. Dür, 'Multipartite entanglement that is robust against disposal of particles', *Physical Review A*, vol. 63, no. 2, pp. 020303, 1–4, 2001. DOI: https://doi.org/10.1103/physreva.63.020303.

[144] J. K. Stockton, R. van Handel and H. Mabuchi, 'Deterministic dicke-state preparation with continuous measurement and control', *Physical Review A*, vol. 70, no. 2, pp. 022106, 1–11, 2004. DOI: https://doi.org/10.1103/physreva.70.022106.

[145] C. Thiel, J. von Zanthier, T. Bastin, E. Solano and G. S. Agarwal, 'Generation of symmetric Dicke states of remote qubits with linear optics', *Physical Review Letters*, vol. 99, no. 19, pp. 193602, 1–4, 2007. DOI: https://doi.org/10.1103/physrevlett.99.193602.

[146] H. Häffner *et al.*, 'Scalable multiparticle entanglement of trapped ions', *Nature*, vol. 438, no. 7068, 643–646, 2005. DOI: https://doi.org/10.1038/nature04279.

[147] D. B. Hume, C. W. Chou, T. Rosenband and D. J. Wineland, 'Preparation of Dicke states in an ion chain', *Physical Review A*, vol. 80, no. 5, pp. 052302, 1–5, 2009. DOI: https://doi.org/10.1103/physreva.80.052302.

[148] I. E. Linington and N. V. Vitanov, 'Robust creation of arbitrary-sized Dicke states of trapped ions by global addressing', *Physical Review A*, vol. 77, no. 1, 010302(R), 1–4, 2008. DOI: https://doi.org/10.1103/physreva.77.010302.

[149] S. S. Ivanov, N. V. Vitanov and N. V. Korolkova, 'Creation of arbitrary Dicke and NOON states of trapped-ion qubits by global addressing with composite pulses', *New Journal of Physics*, vol. 15, no. 2, pp. 023039, 1–11, 2013. DOI: https://doi.org/10.1088/1367-2630/15/2/023039.

[150] X. Zou, K. Pahlke and W. Mathis, 'Generation of arbitrary superpositions of the Dicke states of excitons in optically driven quantum dots', *Physical Review A*, vol. 68, no. 3, pp. 034306, 1–4, 2003. DOI: https://doi.org/10.1103/physreva.68.034306.

[151] N. Kiesel, C. Schmid, G. Toth, E. Solano and H. Weinfurter, 'Experimental observation of four-photon entangled Dicke state with high fidelity', *Physical Review Letters*, vol. 98, no. 6, pp. 063604, 1–4, 2007. DOI: https://doi.org/10.1103/physrevlett.98.063604.

[152] B. T. Torosov and N. V. Vitanov, 'Arbitrarily accurate variable rotations on the Bloch sphere by composite pulse sequences', *Physical Review A*, vol. 99, no. 1, pp. 013402, 1–10, 2019. DOI: https://doi.org/10.1103/PhysRevA.99.013402.

[153] H. K. Cummins, G. Llewellyn and J. A. Jones, 'Tackling systematic errors in quantum logic gates with composite rotations', *Physical Review A*, vol. 67, no. 4, pp. 042308, 1–7, 2003. DOI: https://doi.org/10.1103/physreva.67.042308.

[154] A. Ardavan, 'Exploiting the Poincaré-Bloch symmetry to design high-fidelity broadband composite linear retarders', *New Journal of Physics*, vol. 9, no. 2, pp. 24, 1–8, 2007. DOI: https://doi.org/10.1088/1367-2630/9/2/024.

[155] M. Al-Mahmoud, H. Hristova, V. Coda, A. A. Rangelov, N. V. Vitanov and G. Montemezzani, 'Non-reciprocal wave retarder based on optical rotators combination', *OSA Continuum*, vol. 4, no. 10, pp. 2695–2702, 2021. DOI: https://doi.org/10.1364/OSAC.439325.

[156] A. Messaadi, M. M. Sánchez-López, A. Vargas, P. García-Martínez and I. Moreno, 'Achromatic linear retarder with tunable retardance', *Optics Letters*, vol. 43, no. 14, pp. 3277–3280, 2018. DOI: https://doi.org/10.1364/OL.43.003277.

[157] A. B. Villaverde, D. A. Donatti and D. G. Bozinis, 'Terbium gallium garnet verdet constant measurements with pulsed magnetic field', *Journal of Physics C: Solid State Physics*, vol. 11, no. 12, pp. L495–L498, 1978. DOI: https://doi.org/10.1088/0022-3719/11/12/004.

[158] X. Chen, B. Lavorel, J. P. Boquillon, R. Saint-Loup and M. Jannin, 'Optical rotary power at the resonance of the terbium $^7F_6 \rightarrow {}^5D_4$ line in terbium gallium garnet', *Solid-State Electronics*, vol. 42, no. 9, pp. 1765–1766, 1998. DOI: https://doi.org/10.1016/S0038-1101(98)00163-4.

[159] H. Yoshida, K. Tsubakimoto, Y. Fujimoto, K. Mikami, H. Fujita, N. Miyanaga, H. Nozawa, H. Yagi, T. Yanagitani, Y. Nagata *et al.*, 'Optical properties and Faraday effect of ceramic terbium gallium garnet for a room temperature Faraday rotator', *Optics Express*, vol. 19, no. 16, pp. 15 181–15 187, 2011. DOI: https://doi.org/10.1364/OE.19.015181.